



Contents lists available at ScienceDirect

Tectonophysics

journal homepage: www.elsevier.com/locate/tecto

An attempt to reconstruct 2700 years of seismicity using deep-sea turbidites offshore eastern Taiwan

Rémi Lehu^{a,b,*}, Serge Lallemand^{a,c}, Gueorgui Ratzov^{c,d}, Nathalie Babonneau^{c,e}, Shu-Kun Hsu^{b,c}, Andrew T. Lin^{b,c}, Laurent Dezileau^{a,c}

^a Géosciences Montpellier, Montpellier University, CNRS, France

^b Department of Earth Sciences, National Central University, Zhongli, Taiwan

^c LIA-D3E, France-Taiwan

^d Univ. Nice Sophia Antipolis, CNRS, IRD, Observatoire de la Côte d'Azur, Géazur UMR 7329, 250 rue Albert Einstein, 06560 Valbonne, France

^e Domaines Océaniques Laboratory, Bretagne Occidentale University, IUEM, France

ARTICLE INFO

Article history:

Received 28 January 2015

Received in revised form 19 February 2016

Accepted 13 April 2016

Available online xxx

Keywords:

Active margin

Offshore eastern Taiwan

Paleoearthquakes

Turbidites

Paleoseismology

Peak ground acceleration

Return time

ABSTRACT

The Taiwan area, where the Philippine Sea Plate collides with Eurasia, is one of the most seismically active areas in the world and has been consequently struck repeatedly by destructive earthquakes. To better constrain the occurrence of large earthquakes, we have conducted two cruises in 2012 and 2013 from which five piston, gravity and box-cores were retrieved from selected sites in targeted areas that contain continuous and accurate turbidite deposition offshore eastern Taiwan. Forty-seven turbidite layers deposited between 675 BC and 1212 AD have been described in the cores with facies varying from silty clay to coarse sand. We modeled each turbidite layer using the sedimentation rate deduced from radiocarbon age measurements performed on planktonic foraminifers. Precise dating based on ^{210}Pb – ^{137}Cs chronology provided ages for the XXth century turbidites. Coring sites' locations, biotic association within turbidites beds and seismic calibration over the instrumental period, suggest that earthquakes are the most likely triggering mechanisms of turbidity currents over the last 2700 years. Calibration of correlations between turbidites and instrumental earthquakes allowed us to determine the minimum magnitude of recorded events ($M_w = 6.8$) and the maximum distance between the epicenter and the slope failure. Turbidites' synchronicity between cores has been tested but results showed that this criterion cannot be used in our study area because of the high level of seismicity, i.e., a $M > 6.8$ earthquake recurrence interval much smaller than the uncertainty on radiocarbon ages. The excellent accuracy of dating allows correlating all the turbidites deposited since 1920 with instrumental earthquakes. For each core, we established a return time ranging between 112 and 147 years for the period pre-1900 and ~27 and 34 years for the period post-1900. The discrepancy between pre-1900 and post-1900 recurrence either suggests, that slope stability varies, with higher slope instability after 1900 possibly due to increased sediment delivery by rivers.

© 2016 Published by Elsevier B.V.

1. Introduction

Since the last decade, the Earth has been the theater of unexpected natural disasters such as the December 2004 Sumatra–Andaman earthquake ($M_w 9.1$), the March 2011 Tohoku–Oki earthquake ($M_w 9.0$) and their associated destructive tsunamis. These disasters dramatically highlighted the gap that still exists in the understanding of large earthquakes and associated hazards occurring along subduction zones. Questions remain regarding the seismic potential of subduction zones and the frequency of such large events.

Paleoseismology has proved to be a powerful tool in assessing the occurrence and frequency of large ($M_w > 7$) earthquakes in

continental and coastal domains. Recent advances in the characterization of gravity processes in subaqueous environments and in dating of the sedimentary archive have allowed the development of subaqueous paleoseismology, based on the identification of sedimentary events (such as turbidites) induced by earthquakes. Submarine paleoseismology, and especially turbidite paleoseismology, have provided reliable constraints on the recurrence intervals and spatial distribution of large earthquakes. This method has been successfully tested along tectonically active margins (Adams, 1990; Goldfinger et al., 2007, 2003, 2012; Goldfinger, 2011; Huh et al., 2004; Noda et al., 2008; Gràcia et al., 2010; McHugh et al., 2011; Polonia et al., 2013; Poudroux et al., 2012, 2014; Barnes et al., 2013; Ratzov et al., 2015).

Strong seismic ground shaking is one of the triggers for submarine slope failures (Heezen and Ewing, 1952; Locat and Lee, 2002; Piper and Normark, 2009; Cattaneo et al., 2012; Hsu et al., 2008) that can

* Corresponding author at: Géosciences Montpellier, Montpellier University, France.
E-mail address: lehu.remi@gmail.com (R. Lehu).

evolve downslope into turbidity currents (Mulder and Cochonat, 1996). Other processes than earthquakes could also be responsible of turbidity current generation and the discrimination between different triggering mechanisms still remain ambiguous despite detailed sedimentological characterization (Gorsline et al., 2000; Nakajima and Kanai, 2000; Shiki et al., 2000; Lallemand et al., 2015) have shown that multi-source extreme events, involving earthquakes, submarine landslides and typhoons, can be recorded along the eastern margin of Taiwan. However, synchronous turbidites deposited in independent sedimentary systems over a large area require a regional trigger, most likely a large earthquake (Adams, 1990; Goldfinger et al., 2003, 2007). When available, correlation with historical and instrumental records of earthquakes corroborates the interpretation of the coseismic trigger of turbidity currents.

The continental slope eastwards from the Taiwan mountain belt is characterized by a high sediment supply (Liu et al., 2008), and intense tectonic and seismic activity (Malavieille et al., 2002; Wu et al., 2010; Lallemand et al., 2013). This area concentrates gravity flow sedimentary processes and records successions of turbidites in various sedimentary systems (Lehu et al., 2015). In the northern part, offshore eastern Taiwan, Huh et al. (2004) demonstrated that the four turbidites of the twentieth century are all correlated with four >7 earthquakes. This study offers a field validation of turbidite paleoseismology on this margin, but lacks the spatial and temporal resolution to assess the earthquake hazard of eastern Taiwan currently based on the relatively short period of instrumental earthquakes catalog (~100 years).

In the present paper, we aim (1) to establish the first late Holocene earthquake record of eastern Taiwan, and (2) to estimate the recurrence and magnitude of earthquakes responsible for turbidites deposition. To reach these objectives, we use morphological and sedimentological observations, chronological correlation and hypotheses on peak ground acceleration threshold able to destabilize the submarine slopes.

2. Regional settings

2.1. Geological and seismic context

Taiwan is located in the transfer zone between two opposite verging subductions (Tsai et al., 1977; Wu, 1978). South of the island, the Eurasian Plate (EP) is subducting eastwards beneath the Philippine Sea Plate (PSP), whereas east of Taiwan, the PSP is subducting northwards under the EP along the Ryukyu Trench (Fig. 1). Considering a fixed EP, the PSP converges northwestwards at a rate of 8.1 cm yr^{-1} (Yu et al., 1997). Taiwan results from the collision between the passive continental margin of the South China Sea and the Luzon Volcanic Arc associated with the Manila Subduction (Biq, 1972; Chai, 1972; Malavieille et al., 2002) (Fig. 1). The subsequent deformation is characterized by a very high rate of seismicity onland, but also offshore east Taiwan (Kao et al., 1998). More than 20 $M_w \geq 7$ earthquakes struck this island during the last 100 years but no historical $M_w 8$ earthquake was recorded by the local seismic network (Theunissen et al., 2010). Seismicity concentrates in some very active areas such as the foothills in the western part of the orogen delimited by the deformation front (DF on Fig. 1) (e.g., 1999 $M_w 7.6$ Chichi Earthquake), the Coastal Range which is an extinct segment of the Luzon volcanic arc (LVA) colliding with the orogen (e.g., 1951 $M_w 7$ earthquakes triplet, see Fig. 1A and Table 1), the coastal region north of the Coastal Range is also extremely seismic as well as the E–W-trending South Okinawa Trough (Fig. 1B). Table 2 provides a list of pre-1900 earthquakes described in the literature (Tsai, 1985; Nakamura, 2009; Hsieh and Rau, 2009) that have occurred offshore the eastern Taiwan.

2.2. Sedimentary processes

The eastern Taiwan submarine slope is characterized by a complex morphology. The slope displays steep gradients (15 to 20°). It is deeply

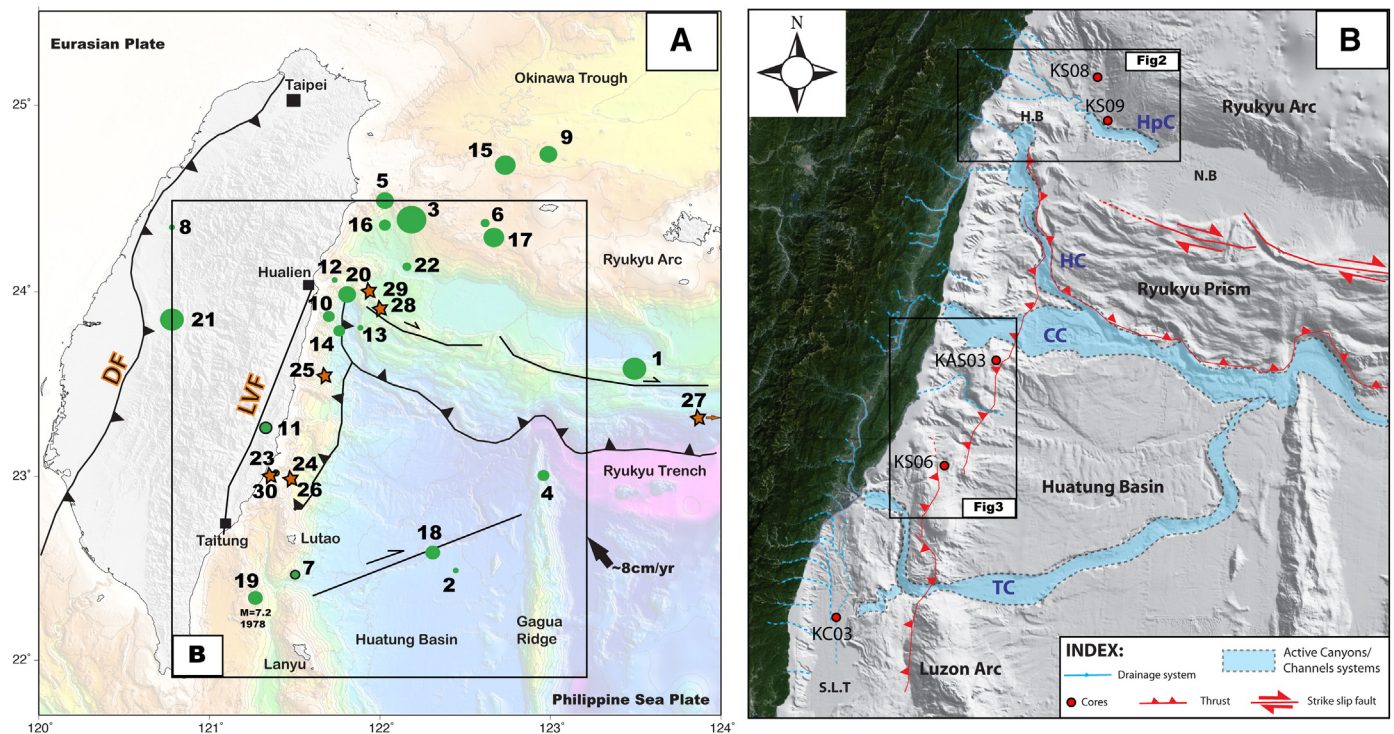


Fig. 1. A: General geodynamic setting of Taiwan. Onland are represented the two major fault zones are DF: Deformation Front and LVF: Longitudinal Valley Fault. The black arrow shows the plate convergence component. Green dots represent the instrumental seismicity over the 20th century with corresponding numbers listed in Table 1. Red stars indicate estimated locations of known paleoearthquakes (numbers listed in Table 2); B: morpho-tectonic map of the study area. Blue dashed-lines represent drainage systems from rivers to offshore channels. In blue are represented the major submarine canyon east Taiwan. Red dots represent the coring sites locations. SLT = Southern Longitudinal Trough; TC = Taitung Canyon; CC = Chimei Canyon; HC = Hualien Canyon; HpC = Hoping Canyon; N.B = Nanao Basin; H.B = Hoping Basin. (For interpretation of the references to color in this figure legend, the reader is referred to the web version of this article.)

Table 1

$M_w \geq 6.8$ earthquakes recorded over the instrumental period (20th century) in the studied area. References for the location origin: 1. (Engdahl and Villaseñor, 2002); 2. (Theunissen et al., 2010); 3. (Cheng and Yeh, 1989); 4. (Chen and Tsai, 2008; Cheng et al., 1996); 5. (Wu et al., 2008).

Eq. number	Date (yy/mm/dd)	Lon. (°)	Lat. (°)	Depth (km)	M_w (*)	Source
1	1915/2/28	123.50	23.60	0	7.5	1
2	1919/12/20	122.50	22.50	35	6.9	1
3	1920/6/5	122.22	24.29	35	7.7	2
4	1921/4/2	123.00	23.00	35	7.1	1
5	1922/9/1	122.04	24.50	35	7.3	1
6	1922/9/14	122.64	24.370	35	7	1
7	1935/9/4	121.55	22.50	20	7	3
8	1935/4/20	120.82	24.35	5	6.9	3
9	1947/9/26	123.00	24.75	110	7.3	1
10	1951/10/21	121.72	23.87	4	7.1	4
11	1951/11/24	121.35	23.27	36	7.1	4
12	1951/10/22	121.72	24.07	1	6.9	4
13	1951/10/22	121.95	23.82	18	6.9	4
14	1957/2/23	121.80	23.80	30	7.1	3
15	1959/4/26	122.79	24.68	126	7.5	1
16	1963/2/13	122.06	24.35	35	7.1	1
17	1966/3/12	122.69	24.30	28	7.5	1
18	1972/1/25	122.32	22.54	10	7.3	1
19	1978/7/23	121.32	22.35	6	7.2	3
20	1986/11/14	121.83	23.99	15	7.3	3
21	1999/9/20	120.80	23.85	6	7.6	5
22	2002/3/31	122.16	24.16	16	7	5
23	2003/12/10	121.38	23.07	21	6.8	5

(*) M_w : equivalent moment magnitude determined by Theunissen et al. (2010).

incised by systems of gullies and canyons (Fig. 1B). The submarine slope also exhibits seafloor escarpments associated with tectonic features such as thrusts and folds (Malavieille et al., 2002). The drainage systems involve three major submarine canyons collecting the sedimentary discharge from the Central Range and the Coastal Range (Fig. 1B). This area is characterized by a variety of sedimentary facies and erosional sedimentary processes from submarine landslides to turbidity currents. The sedimentation is mostly characterized by alternation of turbidites and hemipelagites. Fine-grained turbidites are deposited on mid-slope basins whereas massive turbidites are mainly deposited in turbiditic systems. According to the morpho-sedimentary systems and the sedimentological signatures of the turbidite sequences, the controlling factors of recent sedimentation are related to tectonic and climatic forcing (Lehu et al., 2015).

3. Materials and methods

3.1. Core site location

This study is based on the detailed sedimentary analysis and turbidite correlation in three piston cores, one gravity core, and one box-core acquired during the OR1–1013 (September 2012) and the

Table 2

Historical pre-1900 earthquakes felt along the eastern coast of Taiwan: 1) based on mass mortality of intertidal organisms supposed to result from coseismic coastal uplift after Hsieh and Rau (2009); 2) based on tsunami data after Nakamura (2009); 3) based on historical intensity records after Tsai (1985).

Eq. number	Date (yr. AD)	Lon. (°)	Lat. (°)	Magnitude	Source
24	790–880	121°25' ± 15'E	23° ± 10'N	>7	1
25	1030–1070	121°35' ± 15'E	23°30' ± 30'N	≥7.3	1
26	1260–1290	121°25' ± 15'E	23° ± 10'N	>7	1
27	1771/4/24	124°36'E	23°12'N	8	2
28	1811/3/17	121°48'E	23°48'N	7.5	3
29	1815/10/13	121°42'E	24°N	7.7	3
30	1882/12/9	121°24'E	23°N	7.5	3

OR1–1048 (August 2013) surveys onboard the Taiwanese R/V Ocean Researcher I (see Table 3). As discussed by Lehu et al. (2015), the cores have been strategically selected to characterize the sedimentary depositional areas, where the seismic activity is generated. To avoid the record of turbidites triggered by major floods related to frequent typhoons, we located the core sites away from main sedimentary transfer axis of submarine canyons and deep-sea channels that are directly connected to continental input; instead, we favored sites such as isolated terraces and perched basins sheltered from the continental sedimentary paths (Figs. 1B, 2 and 3).

We defined two zones offshore eastern Taiwan where the cores were retrieved: the Ryukyu forearc basin (hereafter RF) and the Luzon volcanic arc zone (hereafter LA) (Figs. 2 and 3). The cores are termed from north to south: KS09-P and KS08-P (P for piston core) (refer to (Lehu et al., 2015) for cores characteristics), KAS03-P, KS06-B and KS06-G (B for box-core and G for gravity core respectively).

In the RF zone, KS08-P and KS09-P have been collected respectively at 2800 and 2900 m water depth. They are both located on isolated terraces in the Hoping basin (HB in Fig. 1B) at the toe of the northern slope dipping ~11° of the Ryukyu arc (Fig. 2).

About 100 km southward, in the LA zone, KAS03-P was collected at 1700 m water depth on an isolated terrace at mid-slope of a topographic high (Fig. 3). KS06-B, KS06-P and KS06-G have been collected at the same site located at 50 km southward of site KAS03-P, at 1947 m of water depth. This site is located in an isolated perched basin in the eastern slope dipping ~15° of the Luzon arc north of the Lutao volcanic island (Fig. 3).

3.2. Radiometric datings and age models

Radiocarbon dating was performed on 25 samples of hemipelagic sediment bracketing turbidites sequences. For AMS ^{14}C dating, we handpicked between 5 and 11 mg of >250 μm foraminifers. *Orbulina universa* was used because it was the most common species. We also selected *Globigerinoides ruber*, *Globigerinoides bulloides*, *Globigerinoides sacculifer*, and *Globigerinoides conglobatus*. Foraminifers were prepared and dated at the Laboratoire de Mesure ^{14}C (LMC14) on the ARTEMIS accelerator mass spectrometer at the CEA (Atomic Energy Commission) Institute in Saclay (Table 3). To obtain an accurate turbidite event chronology, we calibrate the radiocarbon ages using the Marine13 curve (Reimer et al., 2013) used in the OxCal 4.2 software. For this purpose we need a good estimate of the site-specific offset from the global ocean reservoir, the Delta-R. Offshore eastern Taiwan, based on marine shells, a wide range of reservoir ages have been estimated by Yoneda et al. (2007) and Yu et al. (2010), suggesting fluctuations in the intensity of coastal upwelling and of the oceanographic context (Dezileau et al., 2016). We thus considered in our study the weighted mean value of the ΔR available offshore eastern Taiwan, i.e., 86 ± 40 years (Yoneda et al., 2007).

The next step consisted to accurately determine the age of each single turbidite. Since the collected samples of hemipelagic sediment are located a few cm below or above turbidites, it was necessary to interpolate or extrapolate the ages from sample's depth to turbidite's depth. We used the P_Sequence, a Bayesian model of deposition implemented in the software OxCal 4.2 (Ramsey, 2008) (Fig. 4).

We dated the most recent sedimentary layers using ^{210}Pb , ^{137}Cs methods on the centennial timescale (Fig. 5 and Table 4). These nuclides were determined by gamma spectrometry at the Geosciences Montpellier Laboratory (Montpellier, France). We sampled each centimeter of the box-core KS06-B (36 cm long) and determined the activities of $^{210}\text{Pb}_{\text{ex}}$. This allows to accurately calculate the sedimentation rate and estimate the age of each turbidite event over the last century (Fig. 5) (Dezileau et al., 2016).

Table 3
Location of the studied cores, AMS radiocarbon data and sample age calibrations based on the Marine13 curve.

Core	Longitude	Latitude	Depth (mbsl)	Length (cm)	Sample depth (cm)	¹⁴ C age (yr BP)	Calibrated age (*) (AD except when BC mentioned)					
KS08-P	122°08'	24°19'	2800	91	10–11	940 ± 30	1446–1551					
					34–36	1540 ± 30	962–1127					
					52–54	1675 ± 30	775–900					
					69–71	1530 ± 30	711–834					
					82–84	1540 ± 30	582–692					
KS09-P	122°11'	24°08'	2900	98	0–2	970 ± 30	1435–1505					
					12–13	1415 ± 30	1142–1237					
					21–23	1470 ± 30	1006–1097					
					45–47	1650 ± 30	728–848					
					52–54	1845 ± 30	644–736					
					63–64	286 ± 30	412–557					
					83–85	2305 ± 30	100–220					
					96–98	2550 ± 30	(BC)158–(BC)19					
					KAS03-P	121°42'	23°15'	1700	157	10–12	565 ± 30	1714–1786
										30–32	1310 ± 30	1205–1270
45–47	1405 ± 30	1010–1078										
59–61	1690 ± 30	715–800										
93–95	2130 ± 30	263–363										
126–128	2475 ± 30	(BC)135–(BC)29										
KS06-G	121°30'	22°51'	1947	212	152–154	2885 ± 30	(BC)669–(BC)514					
					26–28	575 ± 30	1829–1877					
					56–58	585 ± 30	1696–1738					
					103–105	1045 ± 30	1319–1371					
					129–131	1365 ± 30	1110–1185					
KS06-B	121°30'	22°51'	1947	36	199–201	1800 ± 30	645–716					

(*) Corrected ages with the local reservoir correction of $\Delta R = 86 \pm 40$ based on (Yoneda et al., 2007).

4. Facies and temporal evolution of turbidite deposition

4.1. Ryukyu forearc

Core KS08-P is 0.91 m-long and composed of clay and silty-clay sediments showing numerous laminations, interpreted as turbidite surges (Fig. 6). We distinguished nine events from 1 to 13.5 cm thick. Their base shows a 12 to 16 μm median grain size, whereas their tails fines upward around 10 μm . XRF data exhibits slightly negative anomalies

of Sr and Ca that anticorrelate Fe anomalies (Fig. 6). Analysis of the grain-size fraction > 150 μm of the basal layers shows ~35% of biogenic content, mostly planktonic foraminifers and sponge spicules (Lehu et al., 2015).

KS09-P is 0.98 m-long, located at the bottom of the northern slope of the Ryukyu arc (Fig. 2). The whole core is composed of clay and silty-clay hemipelagites alternating with fine-grained turbidites. We recognized thirteen turbidites, among which six belong to fine- to medium-grained turbidite facies and are 2 to 10 cm-thick. They are fining

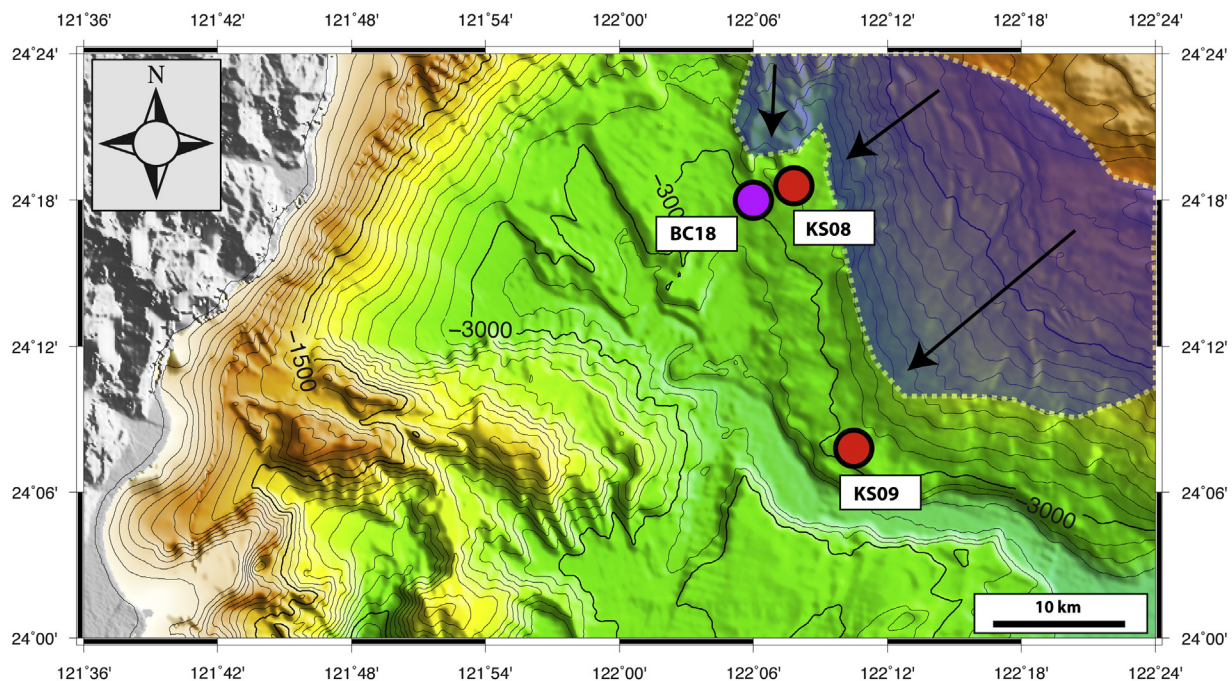


Fig. 2. Close bathymetric view of the Ryukyu forearc zone. Red dots are cores from the present study. Purple dot represents the core location of the study of Huh et al. (2004). Isobaths are represented every 50 m. Purple area represent the turbidite source at corring site. (For interpretation of the references to color in this figure legend, the reader is referred to the web version of this article.)

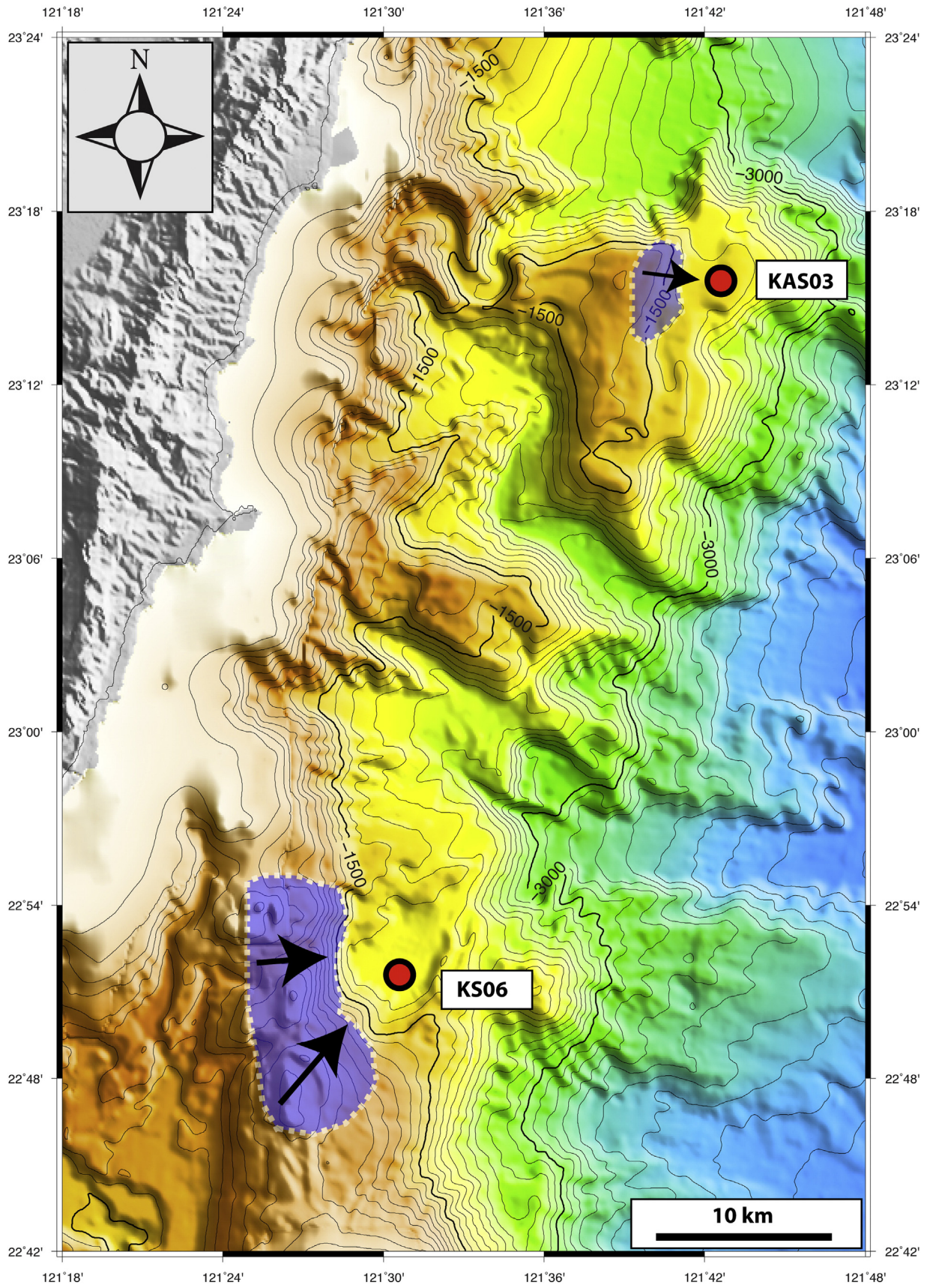


Fig. 3. Bathymetric map representing a zoom on the Luzon volcanic arc zone. Red dots are the cores studied in the present paper. Isobaths are represented every 50 m. Purple area represent the turbidite source at corring site. (For interpretation of the references to color in this figure legend, the reader is referred to the web version of this article.)

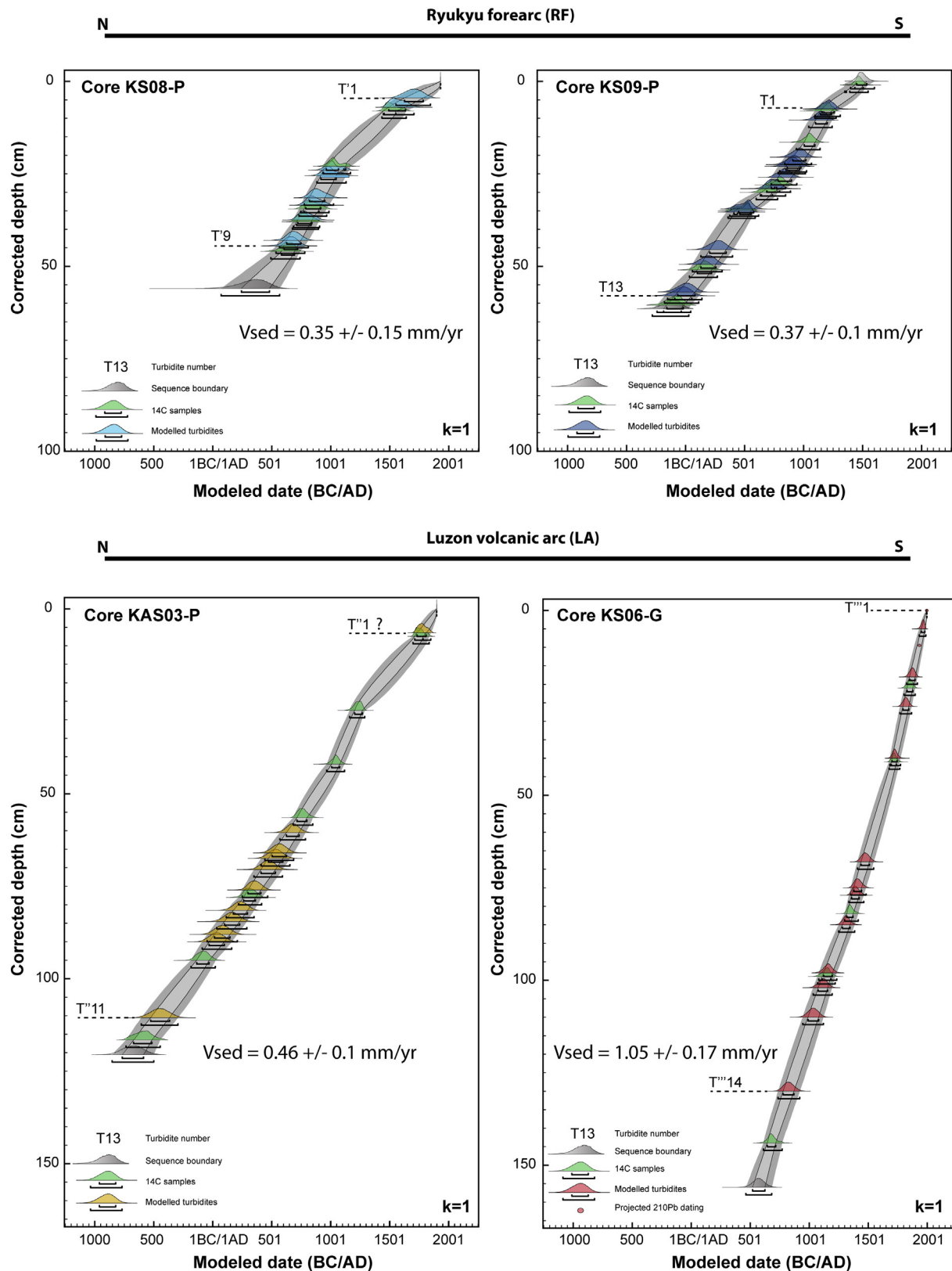


Fig. 4. Oxcal age models from the four studied cores, showing the sedimentation rate of hemipelagite through time and turbidites ages modeled. The k parameter is used to define the regularity of the sedimentation rate along the core. Since hemipelagite is assumed roughly constant rate, the highest k parameter was chosen for each core. All ages are plotted with their 1 and 2σ age range.

upwards constituted by a sharp basal coarse layer (from 17 to 70 μm median grain size) and a silty-clay tail (~ 10 μm median grain size). The seven other events have been interpreted as turbidite surges.

They are characterized by normal grading sequences, with very fine-grained basal layer (~ 12 μm median grain size) and clay tail (~ 10 μm median grain size). The XRF analysis shows slightly positive Sr and Ca

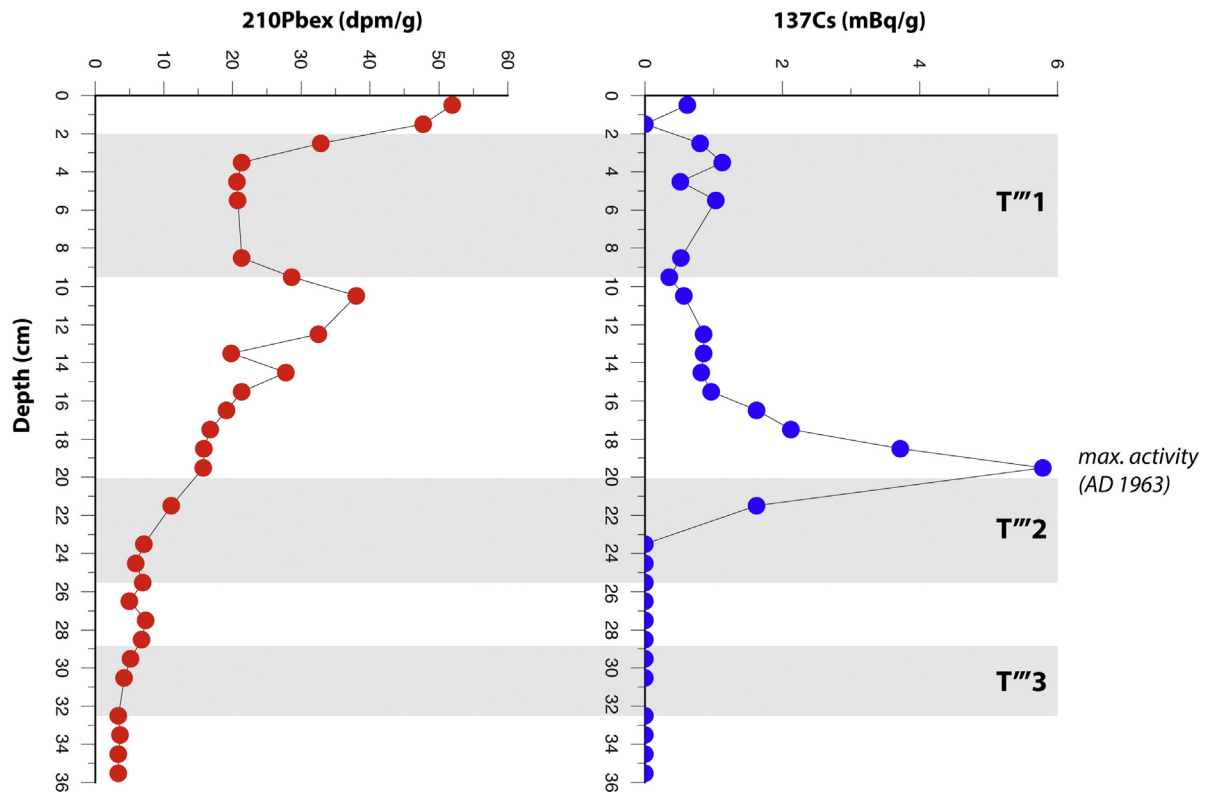


Fig. 5. Activity-depth profiles of Pb and Cs in box-core KS06-B.

anomalies that anticorrelate with slight Fe anomalies (relative to the background sedimentation) (Fig. 6). The coarser fraction of the basal layers reveals a composition of ~30% of biogenic content, mostly planktonic foraminifera and sponge spicules (Lehu et al., 2015).

Table 4
Activity-depth profiles of $^{210}\text{Pb}_{\text{ex}}$ and ^{137}Cs in KS06-B core.

Core depth (cm)	$^{210}\text{Pb}_{\text{ex}}$ (dpm/g)	^{137}Cs (mBq/g)
0.5	51.962	0.621
1.5	47.722	0.000
2.5	32.861	0.804
3.5	21.359	1.125
4.5	20.695	0.514
5.5	20.732	1.030
8.5	21.355	0.522
9.5	28.598	0.359
10.5	37.976	0.567
12.5	32.507	0.852
13.5	19.771	0.852
14.5	27.764	0.822
15.5	21.306	0.964
16.5	19.148	1.629
17.5	16.723	2.123
18.5	15.869	3.718
19.5	15.746	5.793
21.5	11.085	1.624
23.5	7.126	0.000
24.5	5.968	0.000
25.5	6.916	0.000
26.5	4.967	0.000
27.5	7.371	0.000
28.5	6.734	0.000
29.5	5.130	0.000
30.5	4.197	0.000
32.5	3.346	0.000
33.5	3.618	0.000
34.5	3.429	0.000
35.5	3.375	0.000

Cores KS08-P and KS09-P allow to trace turbidites deposited in the Ryukyu Forearc (RF) over the last ~2100 years. The two cores exhibit a ~1150 years overlap from ~350 AD to ~1500 AD. The northernmost site KS08-P contains turbidites T1 to T9 deposited respectively at 1625–1785 AD, 1490–1635 AD, 945–1110 AD, 915–1045 AD, 820–950 AD, 790–915 AD, 720–840 AD, 625–745 AD, 605–720 AD, and 245–480 AD (Fig. 4 and Table 5). Note that no turbidite deposited between ~1100 and ~1500 AD. The most distal site KS09-P records thirteen turbidites (T'1 to T'13), deposited homogeneously during the collected time span, respectively at 1155–1260 AD, 1100–1200 AD, 910–1020 AD, 860–980 AD, 850–965 AD, 785–900 AD, 690–800 AD, 450–580 AD, 410–555 AD, 205–345 AD, 130–255 AD, 65 BC–80 AD, and 90 BC–55 AD (Fig. 4 and Table 5). The mean hemipelagic sedimentation rates for cores KS08 and KS09 are 0.35 ± 0.15 mm/yr and 0.37 ± 0.1 mm/yr respectively. The similarity of the sedimentation rate indicates that the basal erosion of the turbidite beds is negligible.

4.2. Luzon arc

Core KAS03-P is 1.57 m long and contains alternation of clay and silty-clay sediments showing numerous sequences and laminations that differ from the hemipelagic sedimentation (Fig. 7). We identified eleven turbidites interbedded within the hemipelagites. Among them, one 8 cm-thick event (at 118 cm depth below the seafloor) is interpreted as a fine-grained turbidite with a sharp basal silty layer (median grain size $17 \mu\text{m}$) and a fining upward tail (median grain size at top $\sim 10 \mu\text{m}$). We interpret the ten other events as turbidite surges. They are characterized by 2 to 7 cm fining upward sequences with very fine-grained basal layers (ranging from 12 to $16 \mu\text{m}$ median grain size) and clay tail (median grain-size $\sim 11 \mu\text{m}$). The eleven events of KAS03-P are characterized by slight positive Sr and Ca anomalies that are anticorrelated with Fe anomalies (negative relative to the background sedimentation) (Fig. 7). Analysis of the composition of the grain-size fraction $>150 \mu\text{m}$ reveals nearly 30% of biogenic content including mainly planktonic foraminifers and sponge spicules (Lehu

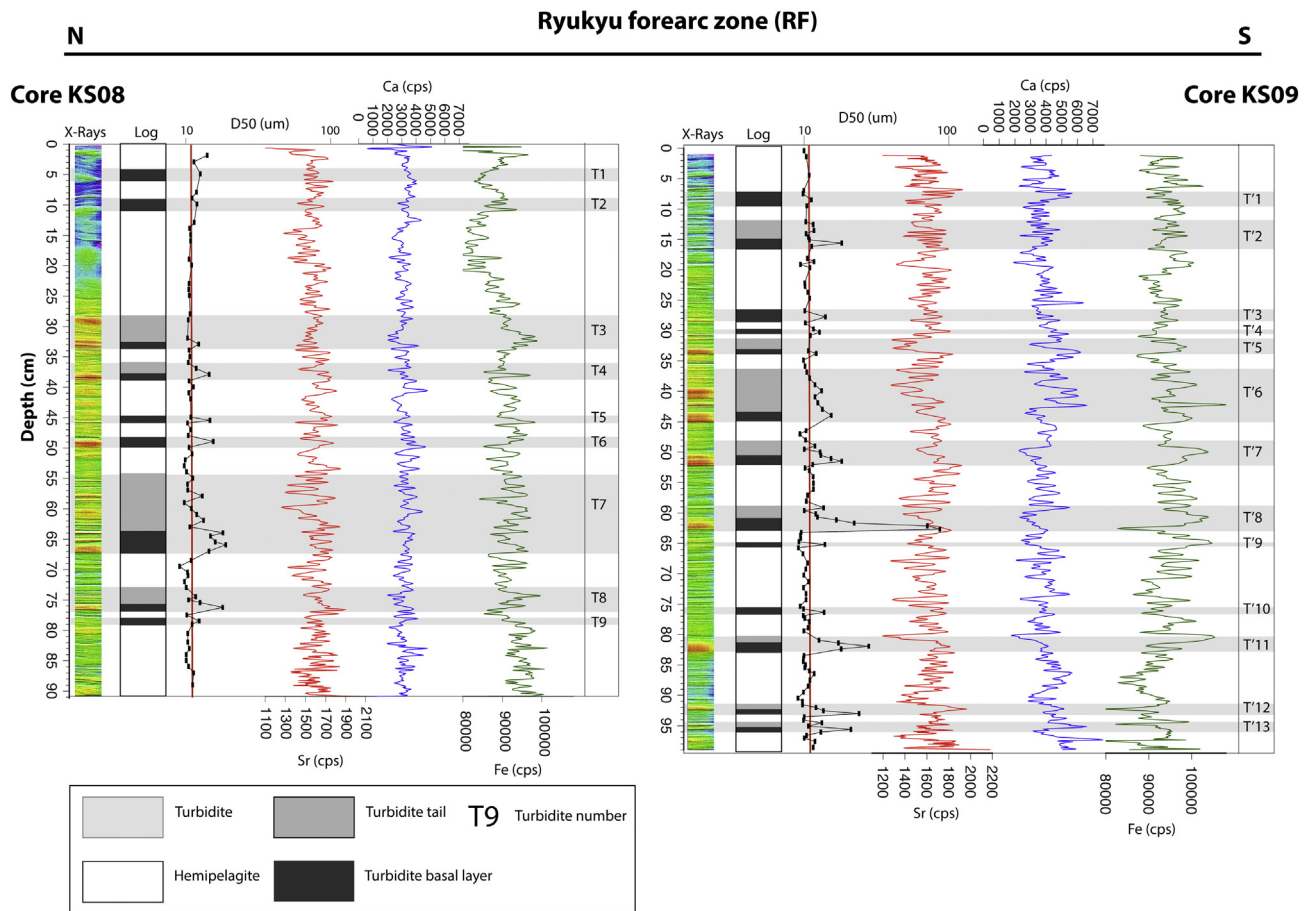


Fig. 6. X-rays imagery (given with equivalent colors of gray tones), lithological description, median grain size, geochemical composition (Sr, Ca and Fe) of the studied sections of the OR1–1013 and OR1–1048 cores from the Ryukyu forearc zone. Turbidite numbers are depicted for each core. Red line marks the 12-m threshold in the grain size. (For interpretation of the references to color in this figure legend, the reader is referred to the web version of this article.)

et al., 2015). Unfortunately, the top 60 cm of the core was disturbed after acquisition and could explain the quasi-lack of turbidites within this interval especially in the bottom of that section (Fig. 7).

Gravity core KS06-G is 2.12 m long. The whole core is composed of clay and silty-clay hemipelagites alternating with fine-grained to coarse-grained turbidites with thicknesses ranging from 2 to 10 cm. The fining upward sequences are characterized by a sharp erosive base with a median grain-size fluctuating from 17 to 200 µm (medium silt to fine sand respectively) and a tail characterized by a median grain size of about 10 µm. XRF data shows clear Sr and Ca positive anomalies, common to all events, that anticorrelate Fe anomalies (Fig. 7). Box-core KS06-B represents the uppermost part of the sedimentary record at that site. It is 36 cm-long and contains three events interbedded with hemipelagites. The two uppermost events are 4 to 8 cm-thick medium-grained turbidites characterized by a base with a median grain size ranging from 20 to 35 µm. The third event, 4 cm thick, is likely attributed to turbidite surge facies and has a base with a median grain size of 13 µm. Like KS06-G, Ca and Sr signals in KS06-B display clear positive anomalies that anticorrelate with Fe anomalies for the two uppermost events, whereas smaller anomalies in Ca and Fe, and a clear positive Sr are observed in the third event (Fig. 7). The biogenic component of the sand grain-size fraction represents nearly 80%, mainly composed by planktonic and benthic foraminifers, and sponge spicules (Lehu et al., 2015). The abundance of the benthic foraminifers represents about 5% of the biotic fraction.

Cores KAS03-P, KS06-G and KS06-B show turbidite deposition in the Luzon Arc (LA) over the last ~2700 years. The two long cores overlap from ~570 AD to ~1900 AD. The slope basin (core KAS03-P) collected eleven turbidites (T^m1 to T^m12) deposited at 1730–1810 AD,

625–735 AD, 505–625 AD, 475–595 AD, 410–530 AD, 300–410 AD, 180–300 AD, 100–230 AD, 15–145 AD, 30 BC–100 AD, and 525–365 BC respectively. The mean hemipelagic sedimentation rate is 0.46 ± 0.1 mm/yr.

The southern slope basin sampled by core KS06-G and KS06-B shows a composite stratigraphic section of fourteen turbidite (T^m1 to T^m14) deposited respectively at 1998–2004 AD (²¹⁰Pb_{ex} and ¹³⁷Cs dating on Fig. 6), 1950–1980 AD (vs 1947–1953 using ²¹⁰Pb and ¹³⁷Cs), 1922–1938 AD (given by the ²¹⁰Pb_{ex} on Fig. 5), 1850–1900 AD, 1795–1845 AD, 1700–1745 AD, 1439–1510 AD, 1380–1445 AD, 1360–1425 AD, 1280–1345 AD, 1120–1195 AD, 1075–1155 AD, 990–1080 AD, 780–870 AD, and 520–625 AD (Fig. 4 and Table 5). Surprisingly, most of the turbidites at site KS06 deposited during a “quiet” period at site KAS03-P, between ~800 AD and ~1650 AD. ²¹⁰Pb_{ex} and ¹³⁷Cs measured in the box-core KS06-B reveal a 2.1 mm/yr hemipelagic sedimentation rate over the last century (Dezileau et al., 2016), whereas radiocarbon age modeling in core KS06-G reveals 1.05 ± 0.17 mm/yr over the last ~1500 years (Fig. 4).

5. Discussion

5.1. Sedimentary sources and turbidite trigger

Large earthquakes are one of the main driving mechanisms for turbidity current generation resulting from the evolution of a slope failure (Piper et al., 1999; Piper and Normark, 2009). Turbidity currents have been used as proxy for paleoearthquakes since the 1929 Grand Banks Earthquake and associated turbidity current (Heezen and Ewing, 1952). However, Adams (1990), proposed that turbidite generation

Table 5

Calibrated ages of the turbidite events. Calibration is based on Marine13 included in OxCal 4.2 calibration software. Turbidite ages are modeled using the P_Sequence model of deposition implemented in OxCal 4.2 (Ramsey, 2008).

Core	Turbidite event	Age min (1 σ)	Age max (1 σ)	
KS08-P	Top	1930	1931	
	T1	1625	1784	
	T2	1491	1634	
	T3	943	1109	
	T4	917	1046	
	T5	820	949	
	T6	788	915	
	T7	720	841	
	T8	627	747	
	T9	604	719	
	Bottom	243	481	
	KS09-P	Top	1451	1535
		T'1	1155	1260
T'2		1102	1201	
T'3		909	1020	
T'4		862	978	
T'5		851	967	
T'6		785	897	
T'7		688	797	
T'8		450	578	
T'9		412	555	
T'10		206	345	
T'11		130	256	
T'12		(BC)65	80	
T'13	(BC)90	53		
Bottom	(BC)185	(BC)36		
KAS03-P	Top	1900	1901	
	T''1	1734	1811	
	T''2	626	734	
	T''3	505	626	
	T''4	474	596	
	T''5	410	532	
	T''6	300	410	
	T''7	176	296	
	T''8	100	230	
	T''9	16	147	
	T''10	(BC)30	100	
	T''11	(BC)524	(BC)365	
	Bottom	(BC)765	(BC)585	
KS06-G/B	Top	2011	2012	
	T'''1	(**)1998	(**)2004	
	T'''2	1950	1980	
	T'''3	(**)1922	(**)1938	
	T'''4	1850	1897	
	T'''5	1794	1844	
	T'''6	1702	1746	
	T'''7	1439	1510	
	T'''8	1378	1443	
	T'''9	1360	1423	
	T'''10	1282	1346	
	T'''11	1122	1196	
	T'''12	1077	1156	
	T'''13	995	1080	
	T'''14	779	870	
Bottom	520	624		

(**) Ages obtained with $^{210}\text{Pb}_{\text{ex}}$ and ^{137}Cs dating.

may be triggered following four mechanisms a) sediment loading, b) wave-induced slumping, c) tsunamis and d) large earthquakes. Post-glacial isostatic rebound (e.g. (Blumberg et al., 2008)) has also been regarded as a possible turbidite triggering mechanism. However, large earthquakes are recognized as the main triggering mechanisms of widespread turbidites in a given region (Goldfinger et al., 2003; Gràcia et al., 2010; Poudroux et al., 2012, 2014; Ratzov et al., 2015).

To support the assumption that our sites mainly record seismic events, we analyzed the biogenic composition of turbidites (fraction $>150\ \mu\text{m}$), to deduce the sedimentary source of turbidites, and more specifically their water depth (Poudroux et al., 2012; Gràcia et al., 2010). The coarse fraction ($>150\ \mu\text{m}$) of the basal layer in cores KS08-P, KS09-P and KAS03-P, is composed of planktonic foraminifers

and sponge spicules (25% of the coarse fraction) (Lehu et al., 2015) supporting a slope origin of turbidites before their transport. This origin is further supported in core KS06, where the coarse fraction contains large amount planktonic foraminifers, sponge spicules and also benthic foraminifers (80% of the coarse fraction) (Fig. 8) (Lehu et al., 2015).

The benthic foraminifers assemblage allows estimating the water depth of the sedimentary sources. It contains the following species (Bassetti, pers. Comm.): *Bolivinita quadrilatera*, *Bulimina aculeata*, *Bulimina costata*, *Bolivinita quadrilatera*, *Bulimina aculeata*, *Cassidulina carinata*, *Cibicides pachyderma*, *Gyroidina sp.*, *Trifarina angulosa*, *Uvigerina proboscidea*. This assemblage supports a water depth located between 200 and 1000 m below the sea level (Bassetti, pers. Comm.). Although benthic foraminifers can be reworked by seafloor erosion during the turbidity current, the fact that the assemblage contains no species living shallower than 200 m implies that turbidites originated below this water depth. In the Taiwan Strait, Nagel et al. (2013) calculated that the typhoon wave base (maximum water depth where fine-grained sediment can be suspended by typhoon waves) corresponds to 50–140 m. The benthic foraminifers assemblage supports that the turbidites originated below the typhoon wave base, and that they are therefore unlikely caused by climatic events. We interpret slope failures leading turbidity currents as most likely triggered by a ground shaking. This interpretation is furthermore supported by the drastically different turbidite composition observed in the Southern Longitudinal Trough (SLT, Fig. 1B). This proximal basin is directly fed by major rivers (Lehu et al., 2015) (such core KC03A located in SLT on Fig.1B and Fig. 8). There, thick and massive sandy turbidites are only composed by lithogenic materials suggesting a direct terrestrial supply from onland rivers to the deep-sea basin during large storm or flood events (Fig. 8) (Lehu et al., 2015).

5.2. Correlation with instrumental seismicity

Numerous earthquakes have been instrumentally recorded in Taiwan since the 20th century, the largest being the 1920 M_w 7.7 earthquake that occurred offshore eastern Taiwan (Fig. 1A, Table 1) (Theunissen et al., 2010).

In the RF area, Huh et al. (2004) have demonstrated that turbidites can be used as a paleoseismicity marker. In box-cores located nearby KS08 site (BC-18 on Fig. 2), four turbidites (1 to 4) (Fig. 9B) are interpreted and dated using $^{210}\text{Pb}_{\text{ex}}$. Among the possible earthquakes candidates shown in Table 1 and Fig. 1, they attributed the four turbidites to the 2002 M'_w 7.0 (where M'_w is the equivalent moment magnitude defined by (Theunissen et al., 2010)), the 1986 M'_w 7.3, the 1966 M'_w 7.5 and the 1922 M'_w 7.0 earthquakes respectively.

We suggest that turbidite 4 in BC-18 (Huh et al., 2004) would be likely attributed to the 1920 M_w 7.7 earthquake (Theunissen et al., 2010) rather than the 1922 earthquake, since its location is closer to the core site BC-18, its magnitude is higher and it occurred prior to the 1922 event.

To associate possible earthquakes to the three most recent turbidites identified in KS06-B (LA area), we aim to calibrate the seismic source responsible for slope instabilities and turbidity currents generation. To do so, we use empirical relationships established by Chung (2013) and methodology developed by Poudroux et al. (2014) that link peak ground acceleration, magnitude and epicentral distance. This relation allows calculating the intensity of the ground shaking (and especially the Peak Ground Acceleration) depending on the distance from the earthquake epicenter. Based on the modeling of ~12,000 accelerograms at ~730 stations in the mountain range installed on rock sites without soil amplification, Chung (2013) has established empirical laws giving PGA as a function of hypocentral distance of shallow moderate to large earthquakes for each magnitude, knowing that the soil sites amplification factor is in the order of 2 to 3.5. For example, a M7 source is responsible for a PGA of 0.03 g at a distance of 50 km for a hard-rock site and ~0.1 g for a soft sediment site. We considered a mean 0.1 g PGA

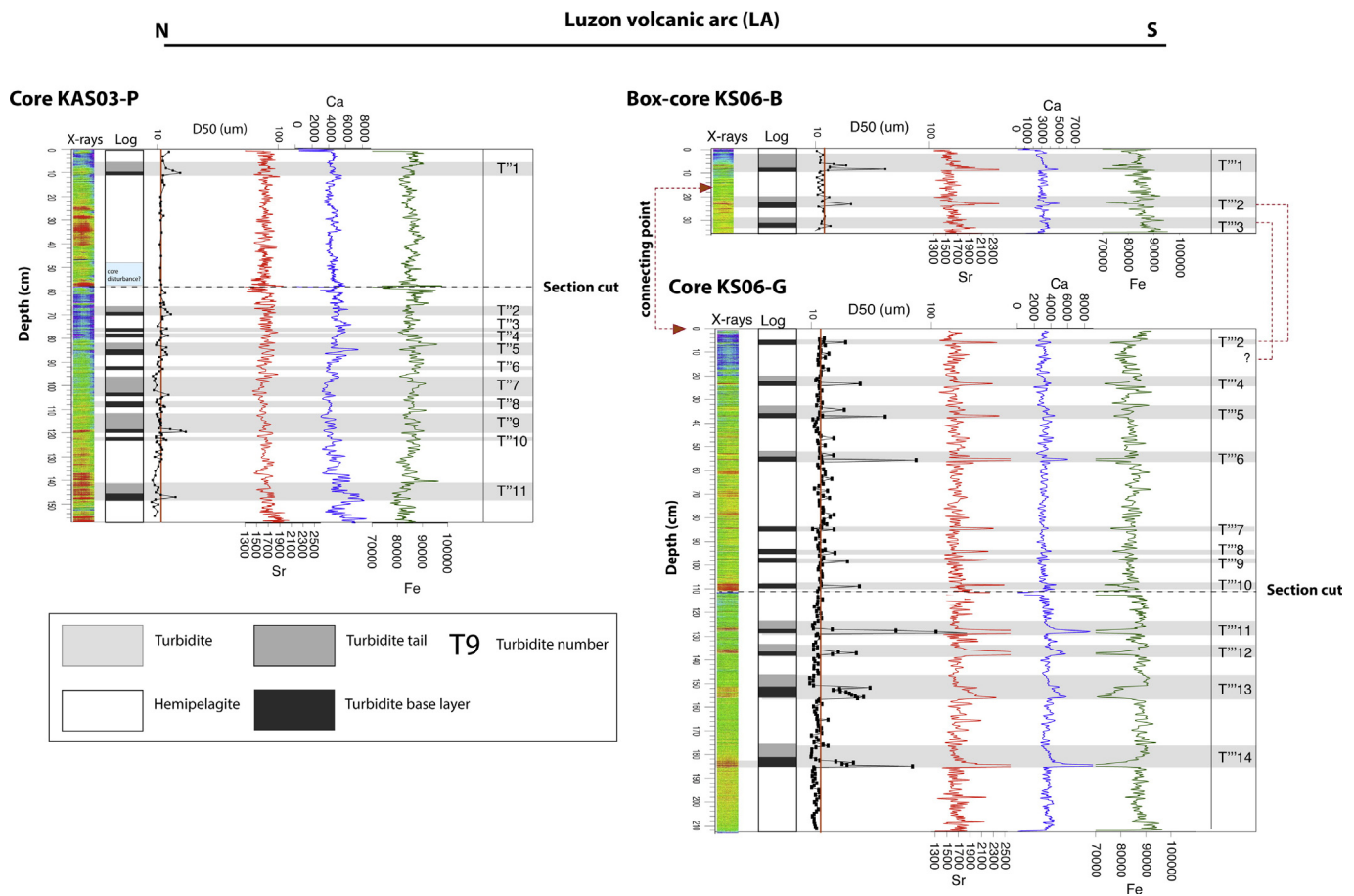


Fig. 7. X-rays imagery (given with equivalent colors of gray tones), lithological description, median grain size, geochemical composition (Sr, Ca and Fe) of the studied sections of the OR1–1013 and OR1–1048 cores from the Luzon volcanic arc zone. Turbidite numbers are depicted for each core. Red line marks the 12-m threshold in the grain size. (For interpretation of the references to color in this figure legend, the reader is referred to the web version of this article.)

value as a threshold for submarine sediment slope failures trigger (Dan et al., 2009; Poudroux et al., 2014). We then test whether an earthquake can generate a PGA strong enough to trigger a slope failure that can evolve into a turbidity current. Considering soft sediments conditions. We calculated that 0.1 g PGA is reached at 50-km epicentral distance for a M_w7 earthquake and at 100-km epicentral distance for a M_w8 earthquake. Therefore, we draw 50-km and 100-km radius circles centered on the turbidites source areas of both sites KS06 and BC-18 (Fig. 10); these circles should encompass the location of any M_w7 and M_w8 earthquakes responsible for the collected turbidites in the cores. As core sites are mostly located in isolated basins surrounded by bathymetric highs, we considered the turbidites as originated from the highest point of the local slope. The inferred source areas are represented in Figs. 2 and 3.

After examination of the catalog of earthquakes along eastern Taiwan (see Table 1), we identified the candidate earthquakes within the source area of KS06 site (Fig. 10). The uppermost turbidite $T''1$ is dated at 2001 ± 3 AD (Dezileau et al., 2016); and correlated with the 2003 M_w 6.8 Chengkong earthquake. This earthquake was located on the submarine slope of the Coastal Range (Fig. 1), about 22 km north of the KS06 site, suggesting a relatively close source and consequently a good candidate for $T''1$. Although the 1999 M_w 7.6 and 2002 M_w 7 earthquakes also both fit the date error bar of turbidite $T''1$, they are however located away from the $PGA > 0.1$ area (earthquakes 21 and 22 in Fig. 9), could not promote slope failures in the source area of $T''1$ and are therefore discarded. $T''2$ is dated at 1950 ± 5 AD; following a similar rationale, the turbidite is correlated with the 1951 M_w 7.1 Taitung earthquake, whereas four M_w 6.9–7.3 earthquakes occurring

in the date error bar are discarded (earthquakes 9 to 13 in Fig. 9). The epicenter of the Taitung earthquake is located inland, on the Coastal Range, about 45 km north of the KS06 site. Finally, $T''3$ is dated at 1928 ± 10 AD and may be correlated with the 1935 M_w 7 earthquake ($N^{\circ}7$ in Fig. 9), while six M_w 6.9–7.3 earthquakes occurring between 1919 and 1935 are discarded. The epicenter is located on the slope of the Luzon arc southward from the Lutao island and about 45 km from the coring site (Fig. 10).

These results show that core sites KS06 and BC-18 can both record $\sim M_w7$ earthquakes within 50-km radius. At a regional scale, one of the most important result of this calculation is that none of the circles of M_w7 and M_w8 of $PGA > 0.1$ g of the two source areas overlap (Fig. 10). Therefore, even if turbidites in cores BC-18 and KS06-B may be temporally correlated within their error bars, they could not have been triggered by the same earthquake. This result is confirmed by the independent earthquake identification by Huh et al. (2004) and this study, showing that events 1 (2002) and $T''1$ (2003), as well as events 4 (1922) and $T''3$ (1935), are related to distinct earthquakes, even if the deposits are radiometrically correlable (see M1, M2 in Fig. 9B). The only possibility to link them to an unique earthquake would be a magnitude $M_w > 8$. Given that such large earthquake has never been recorded during the last century, the paleoseismological approach based on the synchronicity of widespread turbidites, i.e., triggered by large earthquakes (Goldfinger et al., 2003; Gràcia et al., 2010; Poudroux et al., 2014; Ratzov et al., 2015), cannot be applied offshore eastern Taiwan.

This clearly indicates that, if the synchronicity criterion can not be applied for the post-1900 period when ages error bars are minimal

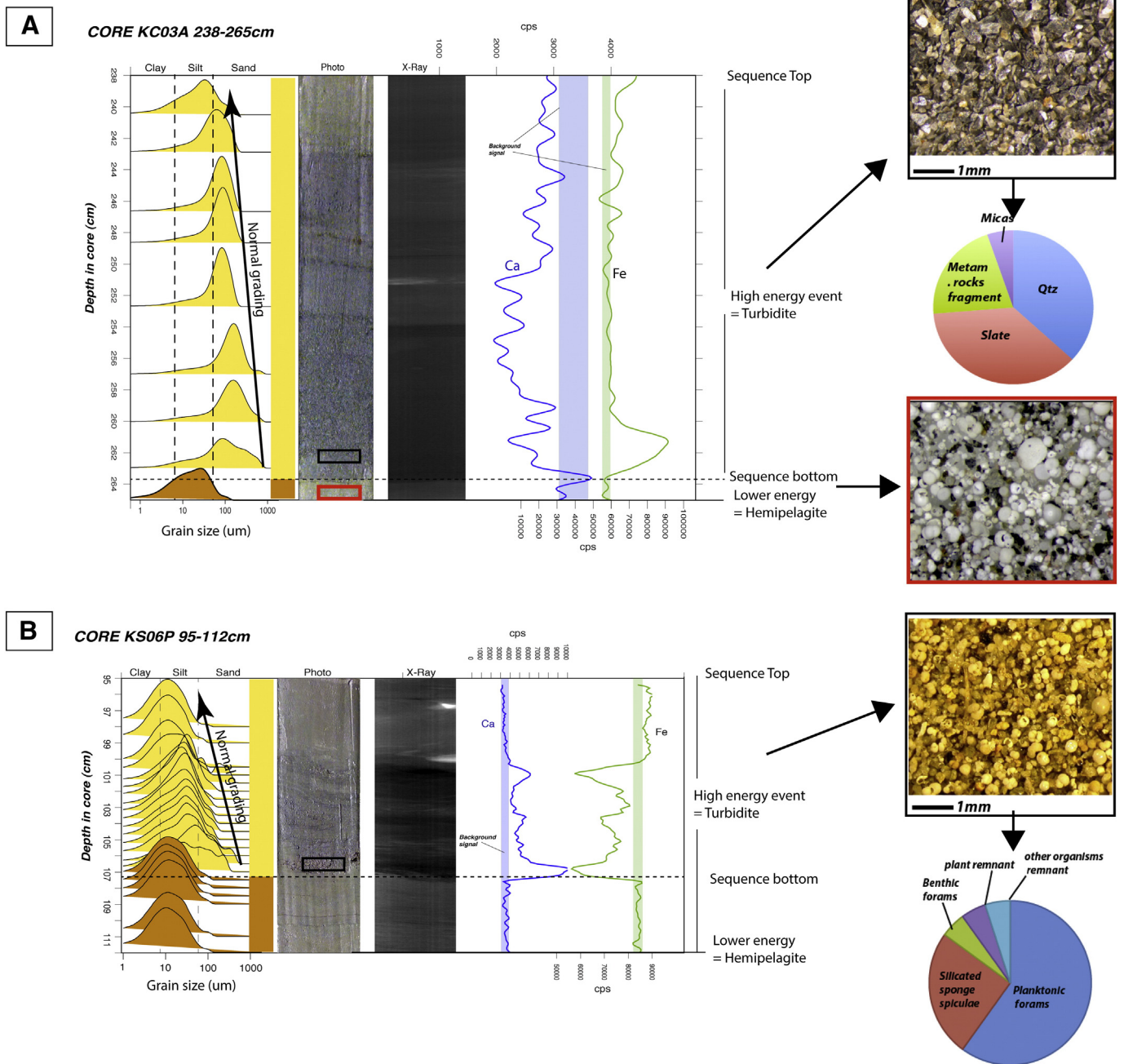


Fig. 8. A. Example of end-member facies of a seismic-driven turbidites from core KS06-P (see location in Fig. 3) showing grain-size distribution, image, X-rays imagery, facies photography, relative composition of the sandy fraction >150 μm and XRF data (Ca and Fe). Blue and green rectangles represent the background signal of XRF data; B. Example of end-member facies of climatic-driven turbidites from core KC03-A in SLT (see Fig. 1B for location) showing the same characteristics as Fig. 8A. (For interpretation of the references to color in this figure legend, the reader is referred to the web version of this article.)

and correlation with historical earthquakes safe, we cannot use it for the pre-1900 period with uncertainties on radiocarbon ages may outpass ± 100 years.

5.3. Estimation of earthquake sources, magnitudes, and recurrence intervals

Applying the same approach as for the instrumental period based on PGA estimation, we extend the method to the pre-1900 period. Our results show that the possibility to trigger margin-scale turbidites in both RF and LA zones would only be a M8 earthquake located offshore Hualien, in a $\sim 120 \times 60$ km ellipsoid area (red overlap in Fig. 10C). This calculation can however not account for turbidites in all the cores, but only in three out of four (either KS06-G, KAS03-P

and KS09-P, or KAS03-P, KS09-P and KS08-P). An even stronger magnitude earthquake would therefore be required to trigger synchronous earthquakes in all the source areas. Based on the detailed tomography of the plates interface offshore Hualien, Lallemand et al. (2013) have concluded that the seismogenic zone west of 123°E was segmented, so that the nucleation of a $M_w \geq 8$ earthquake is unlikely. The calculations show however that $M_w > 7$ earthquakes can account for synchronous turbidites in cores in the RF and LA respectively (gray ellipses in Fig. 10C and D). These results are consistent with the turbidite and instrumental earthquakes correlation for the post-1900 time span.

In the RF, we have considered that core sites mainly recorded earthquake-triggered turbidites between 100 BC and 1800 AD.

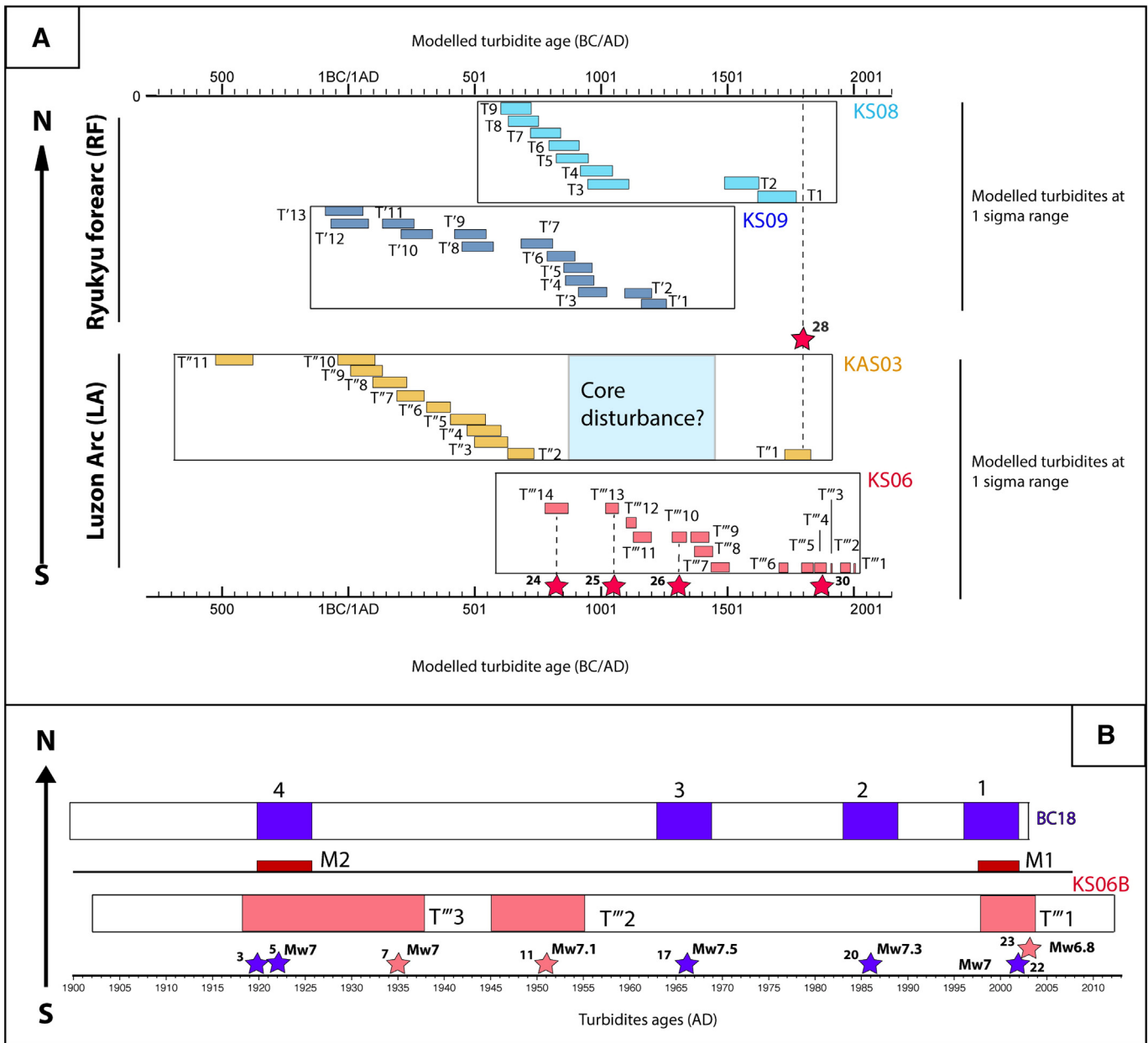


Fig. 9. A. Age range of turbidites from the RF cores and LA cores. Colored rectangles represent turbidites modeled ages at 1 projected on time axis. Stars with most plausible correlations between historical seismic events and turbidites are reported; B. Age correlation over the 20 based on Pb and Cs between box-core BC-18 and KS06-B. Rectangles represent events with their uncertainties projected on time axis. Stars represent candidate earthquakes that may correlate with the turbidite events. In this study, we favor the correlation between event 4 of (Huh et al., 2004) and 1920 M 7.7 event.

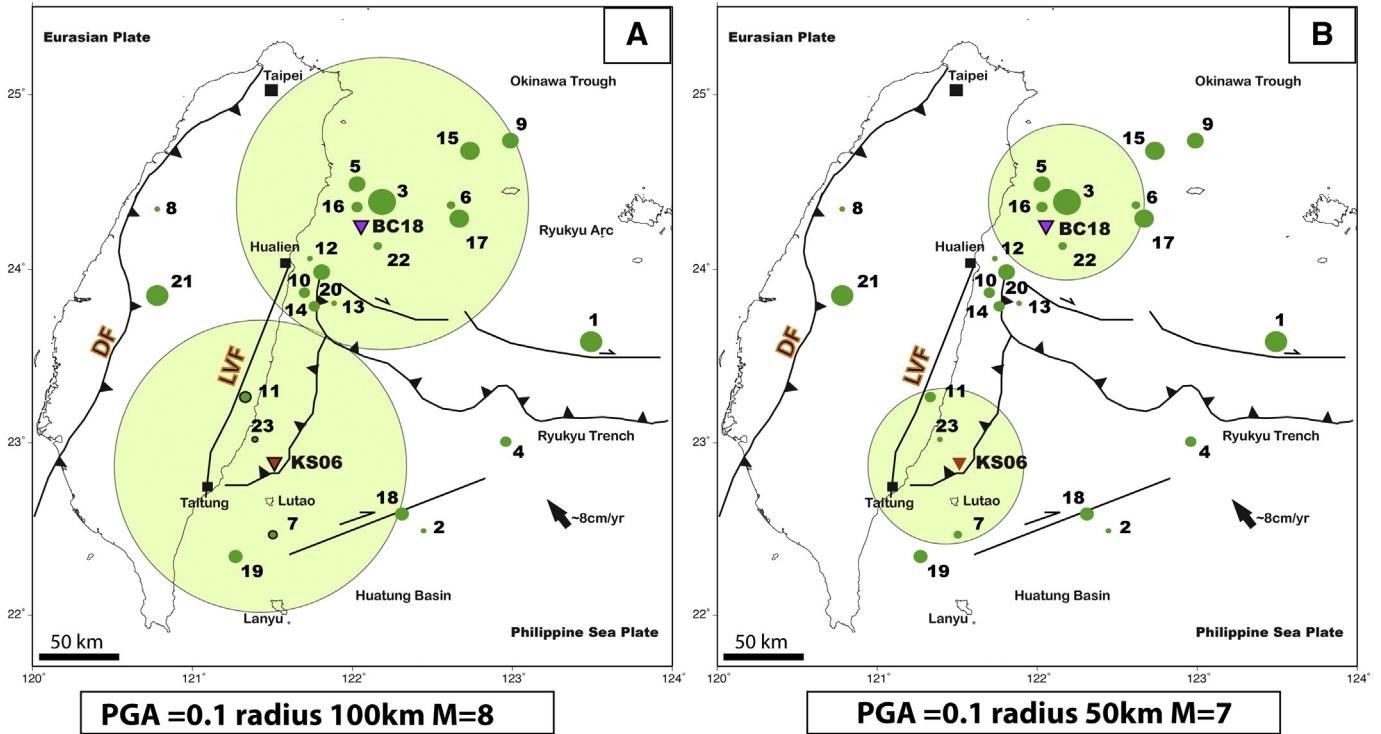
Furthermore, the study of (Huh et al., 2004) revealed that only $7 \leq M_w \leq 7.5$ earthquakes were responsible for turbidites deposition over the last century. This suggests that most of turbidites record in KS08-P and KS09-P are likely to be considered as related to $M \geq 7$. We estimate a recurrence interval of 147 years (period 604–1784 AD) for KS08-P and 112 years (90 BC–1260 AD) for KS09-P.

In the LA area, we considered that turbidites deposition is mainly related to seismic activity between 500 BC to 1900 AD. The results obtained on the instrumental period have shown that all $6.8 \leq M_w \leq 7.1$ earthquakes are likely recorded in box-core KS06-B. We thus estimate a mean recurrence interval for KAS03-P of 125 years for the period 524 BC–734 AD. KS06-G displays continuous turbidites record with clear chemical, grain-size and biotic signatures. Furthermore, the three turbidites layers, recorded in KS06-B, display similar facies and have been correlated to three instrumental earthquakes. It is thus possible to determine a mean recurrence interval only based on turbidites of

KS06-G between 779 AD and 1897 AD, of 112 years for events with magnitude higher than $M_w \geq 6.8$ earthquakes (Table 6).

The recurrence intervals of $M_w \geq 6.8$ earthquakes estimated in both areas for the pre-1900 period are three or four times lower than those occurring during the instrumental period. Indeed, for the RF area, if we consider the six earthquakes that occurred within the black area as drawn on Fig. 10D and considering that BC-18 recorded four events, we estimate a recurrence interval of $M_w \geq 6.8$ of 27 years based on box-core records and 16 years based on instrumental records (Table 6). As such, in the LA area where all events have been recorded by KS06-B, we estimate a recurrence interval of 34 years for $M_w \geq 6.8$ earthquakes, based on the three instrumental earthquakes that occurred within the black zone (Fig. 10D). These higher values obtained for the instrumental period could indicate either that: 1) turbidites do not record all earthquakes, 2) the seismicity was higher there during the last century (Table 6) or 3) climatic conditions during that period

Instrumental seismicity



Historical seismicity

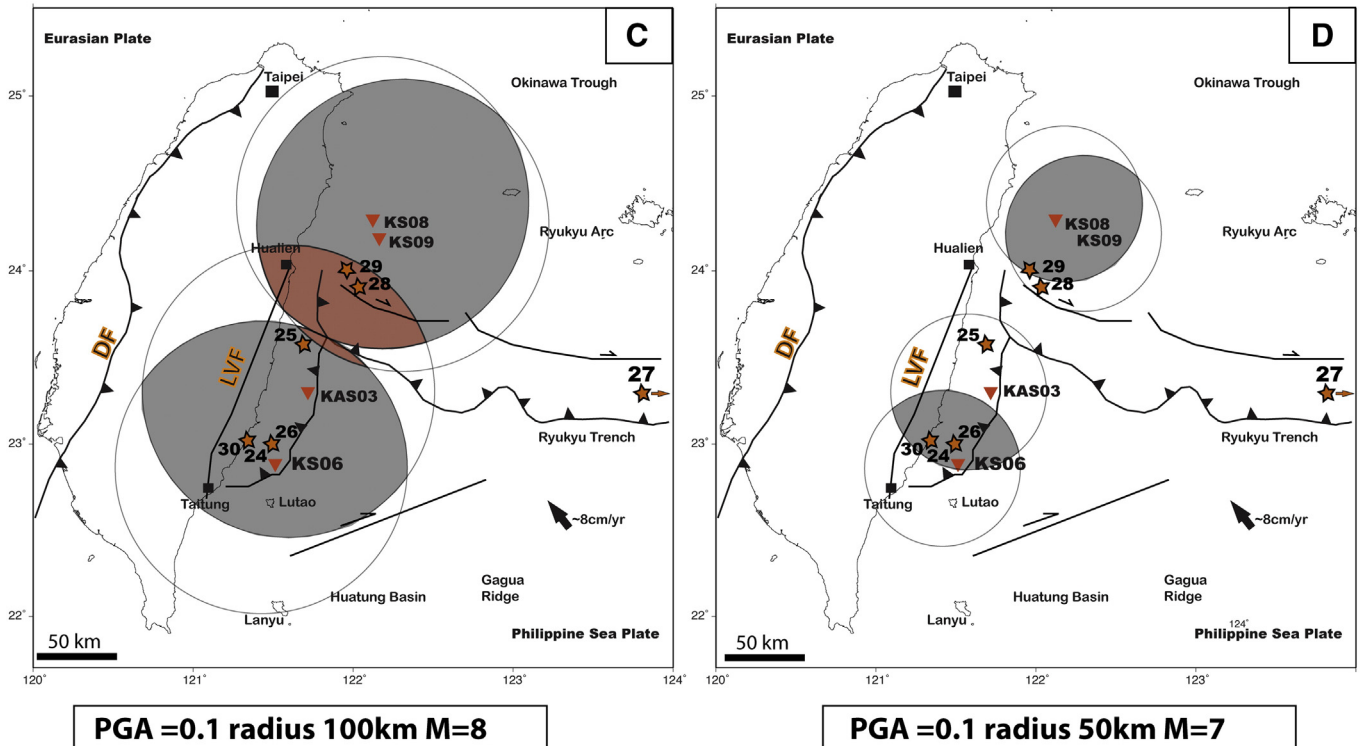


Fig. 10. A. Map showing radius in which an M 8 earthquake will trigger slope failures. Circles have been centered on the turbidite source areas. At 100-km radius peak ground acceleration 0.1 g is reached for such earthquakes. The 0.1 g corresponds to the threshold for slope failures generation. Note that no overlap is possible between the two sites, suggesting that an earthquake M 8 cannot be recorded in both KS06-B and BC-18 cores. Green dots are the seismic event recorded over the instrument period and listed in Table 1; B. Same as A for M 7 earthquake. The value of 0.1 g is reached at 50-km radius. Note that there is no overlap between the two circles, suggesting that it is not possible to record the same M 7 events in both coring sites BC-18 and KS06-B. Reversed triangles represents coring sites. Green dots are the seismic event recorded over the instrument period and listed in Table 1; C. The circles represent the impact of a M 8 earthquake on slope instabilities. They have been drawn around the turbidite source areas. The black areas correspond to the possible local scale events correlations showing the relative areas in which a M 8 earthquake should occurred to trigger synchronous turbidites within a single zone. Red areas corresponds to the overlap of three cores and suggests that to record synchronous turbidites between three cores within the two zones, a M 8 earthquake should occur within this area; D. Same as C but for a M 7 earthquake. We note that regional events cannot be recorded for a M 7. Red stars represent historical earthquakes listed in Table 2. (For interpretation of the references to color in this figure legend, the reader is referred to the web version of this article.)

Table 6

Estimated recurrence interval for $M \geq 6.8$ earthquakes from cores analysis and instrumental records.

Areas	Recurrence interval (in years)			
	Ante-1900		Post-1900	
	Based on cores	Over period	Based on cores	Based on instruments
RF	84 112–147	688–1109 AD 90 BC–1784 AD	27	16
LA	112–125	524 BC–1897 AD	34	34

increased the sediment supply and consequently favored slope instabilities. Indeed, Liu et al. (2001) observed that the frequency of typhoon strikes in Guangdong region, located on the China coast just on the other side of the Taiwan Strait, was much larger during the last century with respect to the last millenium: four versus one event(s) per year. However, they also mentioned that there were two other peaks in the frequency of typhoon occurrences at 1670 ± 10 and 1865 ± 15 AD.

5.4. Historical earthquakes and completeness of the turbidite record

5.4.1. Ryukyu forearc

At least three large earthquakes are reported based on tsunami data (Nakamura, 2009) or historical intensity records (Tsai, 1985) (Fig. 1). Turbidite T1 in core KS08-P dated as 1625–1784 AD and turbidite T¹ in core KAS03-P dated as 1734–1811 AD, may both correlate with the ~M8 1771 earthquake (labeled 27 on Fig. 10 and Table 2) that occurred in the Ryukyu subduction zone and triggered a large tsunami that struck the Yaeyama island (Nakamura, 2009). However, since the epicenter of the 1771 earthquake is located ~200 km from the core KS08-P and ~300 km from core KAS03-P, it remains much beyond the 0.1 PGA area, and is discarded as a trigger candidate. Similarly turbidites T¹ in KAS03-P and T⁵ in KS06-G correlate with the M7.5 earthquake (labeled 28 in Fig. 10 and Table 2) reported in 1811. Its epicenter is located at 120 km away from core KS06-G and thus discard T⁵ as a trigger candidate. However, core KAS03-P is located at 80 km away from the epicenter suggesting that T¹ is likely to be considered as triggered by the 1811 earthquake. Surprisingly, no turbidites correlate with that earthquake in KS08-P or KS09-P, located close to its supposed epicenter suggesting that the turbidite record is incomplete. Finally, the 1815 M7.7 earthquake (labeled 29 in Fig. 10 and Table 2) is also discarded because located too far from KS06 site even if it correlates with T⁵ (1794–1844 AD).

5.4.2. Luzon Arc

At least four earthquakes are documented based on mass mortality of intertidal organisms that are supposed to result from coseismic coastal uplift (Hsieh and Rau, 2009) and historical intensity records (Tsai, 1985).

Turbidite T3 and T4 from KS08-P and T¹³ from KS06-G may both related to the 1030–1070 AD $M \geq 7.3$ earthquake (labeled 25 in Fig. 10 and Table 2). However site KS06 is located closer to the epicenter than site KS08 suggesting that T¹³ from core KS06-G is likely to be considered as triggered by the 1030–1070 AD earthquake. The 1260–1290 AD earthquake (labeled 26 in Fig. 10 and Table 2) could correspond to turbidite T¹⁰ from core KS06-G located about 20 km from the epicenter. Finally the most recent historical earthquake was reported in 1882 AD (labeled 30 in Fig. 10 and Table 2) with magnitude M_w 7.5. Only T⁴ from KS06-G dated as 1850–1897 AD, shares the same time overlap and likely correlates with that earthquake, since its epicenter is located at a short distance from KS06-G core (Fig. 10).

Correlations with historical earthquakes in both areas show that the turbidite record is relatively incomplete, mainly because of the great distance between epicenters and turbidite source areas. As shown with the instrumental seismicity, this result supports that the correlation cannot be solely based on the age fit between

turbidites' dating bars and earthquake dates, but the PGA and epicentral distances need to be taken in account. Finally, the fact that numerous turbidites are not associated to any historical earthquake suggests that they might be triggered by lower magnitude earthquakes located offshore, which did not necessarily induce large damage or casualties in populated zones and where not recorded in historical archives.

5.5. Limitations of turbidite paleoseismology offshore Taiwan

While turbidite paleoseismology revealed to be a powerful tool to record large magnitude earthquakes in subduction zones (Goldfinger et al., 2003; Polonia et al., 2013; Pouderoux et al., 2014) or at diffuse plate boundaries (Gràcia et al., 2010; Ratzov et al., 2015); this study shows some of the limitations of the approach, as only 4 out of over 23 $M_w > 6.8$ earthquakes were retrieved in the turbidite record since 1915. We suggest here some of the limiting factors that could explain the difficulty to obtain a good paleoseismological record with turbidites offshore Taiwan:

- Frequency of earthquakes

Given the unique geodynamical setting along Taiwan, with two opposite verging fast rate subductions (Tsai et al., 1977; Wu, 1978), the seismicity rate is one of the highest in the world, and $M_w > 6.8$ may be separated by few years only, and even couple of months (Table 1). As turbidite paleoseismology relies on the trigger of submarine slope failures, a sufficient amount of sediment prone to failure during earthquakes is required. Even though Taiwan shows the highest land erosion rates and thus sediment supply offshore, it seems unlikely that the sediment buffer could be reloaded enough during such short time spans in-between earthquakes. This is exemplified by the deposit of a single turbidite dated at ~1920 by Huh et al. (2004) whilst an earthquake occurs in the same source area in 1922.

- Magnitude and location of earthquakes

Correlation with known earthquake is probably the safest way to establish the seismic trigger of a turbidite (Sumner et al., 2013), nevertheless, the synchronicity test is robust (Goldfinger et al., 2003), based on the synchronous trigger of turbidity currents over a large area (hundreds of km) together with a recurrence interval for major "recordable" earthquakes larger than 200 years typically as imposed by radiocarbon dating uncertainties. We have proved above that chronologically undistinct (1999–2003) turbidites in different cores have been attributed to different seismic events. Furthermore, to produce a sufficient PGA over such large area, great magnitude earthquake (M_w 8 or more) are required (cf Section 5.2). Given the segmentation of the seismogenic zone in Taiwan inferred by tomography (Lallemand et al., 2013) such great magnitude do probably not occur, thus making difficult the application of the synchronicity test. Our results showed that even if turbidites appear synchronous within their error bars, distinct earthquakes linked to different seismogenic zones triggered them.

- Variation of weathering and sediment supply

To discuss the variability of paleo-earthquake frequencies, the earthquake magnitude threshold for turbidity current trigger needs to remain stable during the time span of the investigation, otherwise one discusses frequencies for different ranges of earthquake magnitudes. Variation of sediment supply to the margin induces changes of this threshold. To prevent such shift, the time span of turbidite paleoseismology investigations is usually limited to stable sediment supply conditions, classically during the sea level highstand (Goldfinger et al., 2003; Gràcia et al., 2010; Ratzov et al., 2015) and homogeneous climatic conditions (Ratzov et al., 2015). Although limited to the highstand sealevel, our results covering the last 2700 years show ~4 times higher turbidite frequencies since 1900. These variations appears correlated with intensification of typhoons and monsoon in Eastern Asia that likely favors the onland erosion,

sediment supply, and therefore should decrease the earthquake magnitude threshold necessary to trigger slope instabilities.

6. Conclusion

Our study is a first attempt to characterize the Late Holocene paleoseismicity over the whole eastern offshore margin of Taiwan. Despite the difficulties in data acquisition, we were able to exploit five cores covering 2700 years. From our detailed investigation, we can mention some important issues:

1. We confirm the potential of turbidite paleoseismology along Taiwan margin despite the intense seismic activity and the influence/imprint of climate in turbidite successions.
2. The synchronicity criterion can not be used in our study area because of the high level of seismicity, i.e., a $M > 7$ earthquake recurrence interval much smaller than the uncertainty on radiocarbon ages.
3. We verified on two box-cores recording the instrumental period that sediments have recorded $6.8 \leq M_w \leq 7.7$ events within a range of 50 km around the source area of turbidites with a recurrence interval of 27 years for BC-18 and 34 years for KS06-B.
4. The turbidite record appears incomplete because of the extremely high seismicity rate, which most likely prevents the buffer of sediment prone to fail to be reloaded.
5. Surprisingly, the pre-1900 recurrence interval of events in individual cores ranges between 84 and 147 years, whereas the post-1900 recurrence interval is 16–34 years. Such discrepancy may also indicate that slope stability varies, with higher values possibly due to an increased sediment delivery by rivers that could be explained by an intensification of storms during the last century.

This study shows some of the limitations of the turbidite paleoseismology method that is classically applied in more simple tectonic contexts, and with lower seismicity rates. Our results provides precious information that will allow to take cautions for further investigations and improve the evolving turbidite paleoseismology discipline.

Acknowledgments

We thank: Maria-Angela Bassetti (CEFREM, Perpignan) for benthic forams identification and interesting discussions, Kuo-Yen Wei (NTU) for XRF analyses, Lee Teh-Quei (IES) for MSCL measurements, TORI staff for core management, Shun-Wen Yu (NCU, Taiwan), Mo-Tsi Tsai (NCU, Taiwan), Don Su (NTU, Taiwan), Lionel Siame, Chris Goldfinger, Jean-Pascal Dumoulin for ^{14}C dating (ARTEMIS program) and also all other people who offered their help, advice and technical support. We thank the two reviewers Hugo Pouderoux and Jean-Noel Proust for their helpful comments. We are also highly grateful to our supports: FIT, BRT, CNRS-INSU, the National Central University, the MOST and the LIA-ADEPT.

References

Adams, J., 1990. Paleoseismicity of the cascadia subduction zone: evidence from turbidites off the oregon-washington margin. *Tectonics* 9 (4), 569–583.

Barnes, P.M., Bostock, H.C., Neil, H.L., Strachan, L.J., Gosling, M., 2013. A 2300-year paleoearthquake record of the southern alpine fault and fiordland subduction zone, new zealand, based on stacked turbidites. *Bull. Seismol. Soc. Am.* 103 (4), 2424–2446.

Biq, C., 1972. Dual-trench structure in the Taiwan-Luzon region. *Proc. Geol. Soc. China* 15, 65–75.

Blumberg, S., Lamy, F., Arz, H., Echtler, H., Wiedicke, M., Haug, H., Oncken, O., 2008. Turbiditic trench deposits at the south-Chilean active margin: a pleistocene-holocene record of climate and tectonics. *Earth Planet. Sci. Lett.* 268 (3), 526–539.

Cattaneo, A., Babonneau, N., Ratzov, G., Dan-Unterseh, G., Yelles, K., Bracene, R., Mercier De Lepinay, B., Boudiaf, A., Déverchère, J., 2012. Searching for the seafloor signature of the 21 May 2003 Boumerdes earthquake offshore central Algeria. *Nat. Hazards Earth Syst. Sci.* 12 (7), 2159–2172.

Chai, B.H., 1972. Structure and tectonic evolution of Taiwan. *Am. J. Sci.* 272 (5), 389–422.

Chen, K.-P., Tsai, Y.-B., 2008. A catalog of Taiwan earthquakes (1900–2006) with homogenized mw magnitudes. *Bull. Seismol. Soc. Am.* 98 (1), 483–489.

Cheng, S.N., Yeh, Y.T., 1989. Catalog of the earthquakes in Taiwan from 1604 to 1988. *Inst. Earth Sci. Acad. Sin.*

Cheng, S.-N., Yeh, Y.-T., Yu, M.-S., 1996. The 1951 taitung earthquake in taiwan. *J. Geol. Soc. Chin.-Taiwan* 39, 267–286.

Chung, J.-K., 2013. Peak ground motion predictions with empirical site factors using taiwan strong motion network recordings. *Earth Planets Space* 65 (9), 957–972.

Dan, G., Sultan, N., Savoye, B., Deverchère, J., Yelles, K., 2009. Quantifying the role of sandy-silty sediments in generating slope failures during earthquakes: example from the algerian margin. *Int. J. Earth Sci.* 98 (4), 769–789.

Dezileau, L., Lehu, R., Lallemand, S., Hsu, S.-K., Babonneau, N., Ratzov, G., Lin, A.T., S. D., 2016. Historical reconstruction of submarine earthquakes using 210Pb, 137Cs and 241Am turbidite chronology and radiocarbon reservoir age estimation off east taiwan. *Radiocarbon*.

Engdahl, E.R., Villaseñor, A., 2002. 41 global seismicity: 1900–1999. *Int. Geophys.* 81 (665–XVI).

Goldfinger, C., 2011. Submarine paleoseismology based on turbidite records. *Ann. Rev. Mar. Sci.* 3, 35–66.

Goldfinger, C., Nelson, C.H., Johnson, J.E., 2003. Holocene earthquake records from the cascadia subduction zone and northern san andreas fault based on precise dating of offshore turbidites. *Annu. Rev. Earth Planet. Sci.* 31 (1), 555–577.

Goldfinger, C., Morey, A.E., Nelson, C.H., Gutiérrez-Pastor, J., Johnson, J.E., Karabanov, E., Chaytor, J., Eriksson, A., 2007. Rupture lengths and temporal history of significant earthquakes on the offshore and north coast segments of the Northern San Andreas Fault based on turbidite stratigraphy. *Earth Planet. Sci. Lett.* 254 (1–2), 9–27 (Feb.).

Goldfinger, C., Nelson, C.H., Morey, A.E., Johnson, J.E., Patton, J., Karabanov, E., Gutierrez-Pastor, J., Eriksson, A.T., Gracia, E., Dunhill, G., et al., 2012. Turbidite Event History: Methods and Implications for Holocene Paleoseismicity of the Cascadia Subduction Zone. US Department of the Interior, US Geological Survey.

Gorsline, D., De Diego, T., Nava-Sanchez, E., 2000. Seismically triggered turbidites in small margin basins: Alfonso Basin, Western Gulf of California and Santa Monica Basin, California Borderland. *Sediment. Geol.* 135 (1–4), 21–35 (Sep.).

Gràcia, E., Vizcaino, A., Escutia, C., Asioi, A., Rodés, A., Pallàs, R., Garcia-Orellana, J., Lebreiro, S., Goldfinger, C., 2010. Holocene earthquake record offshore Portugal (SW Iberia): testing turbidite paleoseismology in a slow-convergence margin. *Quat. Sci. Rev.* 29 (9–10), 1156–1172 (May).

Heezen, B.C., Ewing, W.M., 1952. Turbidity currents and submarine slumps, and the 1929 grand banks [newfoundland] earthquake. *Am. J. Sci.* 250 (12), 849–873.

Hsieh, M.-L., Rau, R.-J., 2009. Late holocene coseismic uplift on the Hua-Tung coast, eastern Taiwan: evidence from mass mortality of intertidal organisms. *Tectonophysics* 474 (3), 595–609.

Hsu, S.-K., Kuo, J., Lo, C.-L., Tsai, C.-H., Doo, W.-B., Ku, C.-Y., Sibuet, J.-C., 2008. Turbidity currents, submarine landslides and the 2006. *Terr. Atmos. Ocean. Sci.* 19 (6), 762–772.

Huh, C.-A., Su, C.-C., Liang, W.-T., Ling, C.-Y., 2004. Linkages between turbidites in the southern Okinawa Trough and submarine earthquakes. *Geophys. Res. Lett.* 31, 2–5.

Kao, H., Shen, S.-S.J., Ma, K.-F., 1998. Transition from oblique subduction to collision: earthquakes in the southernmost Ryukyu arc-Taiwan region. *J. Geophys. Res. Solid Earth* 103 (B4), 7211–7229 (1978–2012).

Lallemand, S., Theunissen, T., Schnürle, P., Lee, C.-S., Liu, C.-S., Font, Y., 2013. Tectonophysics Indentation of the Philippine Sea plate by the Eurasia plate in Taiwan: details from recent marine seismological experiments. *Tectonophysics* 594, 60–79.

Lallemand, S., Lehu, R., Rétif, F., Hsu, S.-K., Babonneau, N., Ratzov, G., Bassetti, M.-A., Dezileau, L., Hsieh, M.-L., Dominguez, S., 2015. A 3000 years-old sequence of extreme events revealed by marine and shore deposits east of taiwan. *Tectonophysics*.

Lehu, R., Lallemand, S., Hsu, S.-K., Babonneau, N., Ratzov, G., Andrew, T.L., Laurent, D., 2015. Deep-sea sedimentation offshore eastern taiwan: facies and processes characterization. *Mar. Geol.* 369, 1–18.

Liu, K.-b., Shen, C., Louie, K.-s., 2001. A 1000-year history of typhoon landfalls in guangdong, southern china, reconstructed from chinese historical documentary records. *Ann. Assoc. Am. Geogr.* 91 (3), 453–464.

Liu, J., Liu, C.S., Xu, K.H., Milliman, J.D., Chiu, J.K., Kao, S.J., Lin, S.W., 2008. Flux and fate of small mountainous rivers derived sediments into the Taiwan Strait. *Mar. Geol.* 256 (1–4), 65–76 (Dec.).

Locat, J., Lee, H.J., 2002. Submarine landslides: advances and challenges. *Can. Geotech. J.* 39 (1), 193–212.

Malavieille, J., Lallemand, S., Dominguez, S., Deschamps, A., Lu, C., Liu, C., Schnürle, P., Hsu, J., Liu, S., Sibuet, J., et al., 2002. Arc-continent collision in taiwan new marine observations and tectonic evolution. *Geol. Soc. Am. Spec. Pap.* 189–213.

McHugh, C.M., Seebler, L., Braudy, N., Cormier, M.-H., Davis, M.B., Diebold, J.B., Dieudonne, N., Douilly, R., Gulick, S.P., Hornbach, M.J., et al., 2011. Offshore sedimentary effects of the 12 January 2010 haiti earthquake. *Geology* 39 (8), 723–726.

Mulder, T., Cochonot, P., 1996. Classification of offshore mass movements. *J. Sediment. Res.* 66 (1), 43–57.

Nagel, S., Castellort, S., Wetzel, A., Willett, S.D., Mouthereau, F., Lin, A.T., 2013. Sedimentology and foreland basin paleogeography during taiwan arc continent collision. *J. Asian Earth Sci.* 62, 180–204.

Nakajima, T., Kanai, Y., 2000. Sedimentary features of seismoturbidites triggered by the 1983 and older historical earthquakes in the eastern margin of the japan sea. *Sediment. Geol.* 135 (1), 1–19.

Nakamura, M., 2009. Fault model of the 1771 yaeyama earthquake along the Ryukyu trench estimated from the devastating tsunami. *Geophys. Res. Lett.* 36 (19).

- Noda, A., TuZino, T., Kanai, Y., Furukawa, R., Uchida, J.-i., 2008. Paleoseismicity along the southern kuril trench deduced from submarine-fan turbidites. *Mar. Geol.* 254 (1), 73–90.
- Piper, D.J., Normark, W.R., 2009. Processes that initiate turbidity currents and their influence on turbidites: a marine geology perspective. *J. Sediment. Res.* 79 (6), 347–362.
- Piper, D.J.W., Cochonot, P., Morrison, M.L., 1999. The sequence of events around the epicentre of the 1929 Grand Banks earthquake: initiation of debris flows and turbidity current inferred from sidescan sonar. *Sedimentology* 46 (1), 79–97 (Feb.).
- Polonia, A., Panieri, G., Gasperini, L., Gasparotto, G., Bellucci, L.G., Torelli, L., 2013. Turbidite paleoseismology in the Calabrian Arc Subduction Complex (Ionian Sea). *Geochem. Geophys. Geosyst.* 14 (1), 112–140 (Jan.).
- Pouderoux, H., Lamarche, G., Proust, J.-N., 2012. Building an 18 000-year-long paleo-earthquake record from detailed deep-sea turbidite characterisation in Poverty Bay, New Zealand. *Nat. Hazards Earth Syst. Sci.* 12 (6), 2077–2101 (Jun.).
- Pouderoux, H., Proust, J.-N., Lamarche, G., 2014. Submarine paleoseismology of the northern hikurangi subduction margin of new zealand as deduced from turbidite record since 16 ka. *Quat. Sci. Rev.* 84, 116–131.
- Ramsey, C.B., 2008. Deposition models for chronological records. *Quat. Sci. Rev.* 27 (1), 42–60.
- Ratzov, G., Cattaneo, A., Babonneau, N., Déverchère, J., Yelles, K., Bracene, R., Courboulex, F., 2015. Holocene turbidites record earthquake supercycles at a slow-rate plate boundary. *Geology* 43 (4), 331–334.
- Reimer, P.J., Bard, E., Bayliss, A., Beck, J.W., Blackwell, P.G., Ramsey, C.B., Buck, C.E., Cheng, H., Edwards, R.L., Friedrich, M., et al., 2013. Intcal13 and marine13 radiocarbon age calibration curves 0–50,000 years cal bp. *Radiocarbon* 55 (4), 1869–1887.
- Shiki, T., Kumon, F., Inouchi, Y., Kontani, Y., Sakamoto, T., Tateishi, M., Matsubara, H., Fukuyama, K., 2000. Sedimentary features of the seismo-turbidites, Lake Biwa, Japan. *Sediment. Geol.* 135 (1), 37–50.
- Sumner, E.J., Siti, M.I., McNeill, L.C., Talling, P.J., Henstock, T.J., Wynn, R.B., Djajadihardja, Y.S., Permana, H., 2013. Can turbidites be used to reconstruct a paleoearthquake record for the central Sumatran margin? *Geology* 41 (7), 763–766.
- Theunissen, T., Font, Y., Lallemand, S., Liang, W.-T., 2010. The largest instrumentally recorded earthquake in Taiwan: revised location and magnitude, and tectonic significance of the 1920 event. *Geophys. J. Int.* 183 (3), 1119–1133 (Dec.).
- Tsai, Y.-B., 1985. A study of disastrous earthquakes in taiwan, 1683–1895. *Bull. Inst. Earth Sci. Acad. Sin.* 5, 1–44.
- Tsai, Y., Teng, T., Chiu, J., Liu, L., 1977. Tectonic implications of the seismicity in the taiwan region. *Mem. Geol. Soc. China* 2, 13–41.
- Wu, F.T., 1978. Recent tectonics of taiwan. *J. Phys. Earth* 26 (Supplement), S265–S299.
- Wu, Y.-M., Chang, C.-H., Zhao, L., Teng, T.-L., Nakamura, M., 2008. A comprehensive relocation of earthquakes in Taiwan from 1991 to 2005. *Bull. Seismol. Soc. Am.* 98 (3), 1471–1481.
- Wu, W.-N., Kao, H., Hsu, S.-K., Lo, C.-L., Chen, H.-W., 2010. Spatial variation of the crustal stress field along the Ryukyu–Taiwan–Luzon convergent boundary. *J. Geophys. Res. Solid Earth* 115 (B11) (1978–2012).
- Yoneda, M., Uno, H., Shibata, Y., Suzuki, R., Kumamoto, Y., Yoshida, K., Sasaki, T., Suzuki, A., Kawahata, H., 2007. Radiocarbon Marine Reservoir Ages in the Western Pacific Estimated by Pre-bomb Molluscan Shells. *Nuclear Instruments and Methods in Physics Research Section B: Beam Interactions with Materials and Atoms* Vol. 259(1), pp. 432–437.
- Yu, S.-B., Chen, H.-Y., Kuo, L.-C., 1997. Velocity field of gps stations in the taiwan area. *Tectonophysics* 274 (1), 41–59.
- Yu, K., Hua, Q., Zhao, J.-X., Hodge, E., Fink, D., Barbetti, M., 2010. Holocene marine 14c reservoir age variability: evidence from 230th-dated corals in the south china sea. *Paleoceanography* 25 (3).